RADIATIVE CONTOUR MAPPING USING UAS SWARM

By

Zachary Cook

Bachelor of Science in Engineering – Mechanical Engineering
University of Nevada, Las Vegas
2015

A thesis submitted in partial fulfillment
of the requirements for the

Master of Science in Engineering – Mechanical Engineering

Department of Mechanical Engineering
Howard R. Hughes College of Engineering
The Graduate College

University of Nevada, Las Vegas
December 2017

ProQuest Number: 10689898

ProQuest 10689898

Published by ProQuest LLC (2018). Copyright of the Dissertation is held by the Author.

Thesis Approval

The Graduate College
The University of Nevada, Las Vegas

November 17, 2017

This thesis prepared by

Zachary Cook

entitled

Radiative Contour Mapping Using UAS Swarm

is approved in partial fulfillment of the requirements for the degree of

Master of Science in Engineering – Mechanical Engineering
Department of Mechanical Engineering

Woosoon Yim, Ph.D.   Kathryn Hausbeck Korgan, Ph.D.
Examination Committee Chair   *Graduate College Interim Dean*

Alexandar Barzilov, Ph.D.
Examination Committee Member

Mohamed Trabia, Ph.D.
Examination Committee Member

Sahjendrah Singh, Ph.D.
Graduate College Faculty Representative

ii

Abstract

The work is related to the simulation and design of small and medium scale unmanned aerial system (UAS), and its implementation for radiation measurement and contour mapping with onboard radiation sensors. The compact high-resolution CZT sensors were integrated to UAS platforms as the plug-and-play components using Robot Operation System. The onboard data analysis provides time and position-stamped intensities of gamma-ray peaks for each sensor that are used as the input data for the swarm flight control algorithm. In this work, a UAS swarm is implemented for radiation measurement and contour mapping. The swarm of UAS has advantages over a single agent based approach in detecting radiative sources and effectively mapping the area. The proposed method can locate sources of radiation as well as mapping the contaminated area for enhancing situation awareness capabilities for first responders. This approach uses simultaneous radiation measurements by multiple UAS flying in a circular formation to find the steepest gradient of radiation to determine a bulk heading angle for the swarm for contour mapping, which can provide a relatively precise boundary of safety for potential human exploration.

Table of Contents

List of Figures

ix

Chapter 1: Introduction

Unmanned aerial systems (UAS) are being used in increasingly novel ways and in many cases solving problems that were hard to accomplish with other conventional methods. Due to the ability of multirotor UAS to fly close to the ground, it is possible for relatively accurate and detailed mapping [1] to be done using onboard sensors such as LIDAR, cameras and other environmental sensors. Terrain can be shown in three dimensions with accuracy unparalleled when compared to satellite imagery. Surveillance [2] has become a prominent area facilitated by UAS. Persistent surveillance [3] with multi-day missions is also possible due to the unmanned nature of the UAS.

Semi and fully autonomous [4] UAS have the ability to offload much of the cognitive load of the operators when being deployed while accomplishing tasks that would be extremely difficult for a human operator only. The ability to autonomously navigate a given operational area while accomplishing given tasks enables an operator to be free from navigation tasks, and can focus on overall task management.

Recently, the cost of developing multirotor UAS platforms has dropped drastically partly due to the increase in their popularity. This prevalence of low cost UAS allows for the use of multiple UAS simultaneously as a swarm. An emerging application of using an autonomous UAS swarm is radiation detection and mapping in a low-altitude. The benefits of using a UAS swarm rather than a single agent is its ability to get multiple measurements simultaneously in different locations to gather information faster and more efficiently than is possible than with a single UAS.

First responders stand to experience huge benefits from the UAS boom[5]. UAS can be deployed in different emergency events by the first responders whether they are indoor or outdoor including forests, caves, and other near-earth environments along with urban structures such as

1

buildings and tunnels. This also includes UAS for monitoring and maintaining the processes inside of the nuclear power plant (NPP) containment structure to ensure that the plant stays within optimal operating conditions for reliable and efficient power generation. In 2011 in Fukushima, Japan, an earthquake triggered a tsunami which initially disabled the cooling of three of the six reactors at the Fukushima Daiichi nuclear power plant. Following the disaster, UAS were used in order to measure radiation levels [6] to prevent first responders exposing to potential high doses of radiation.
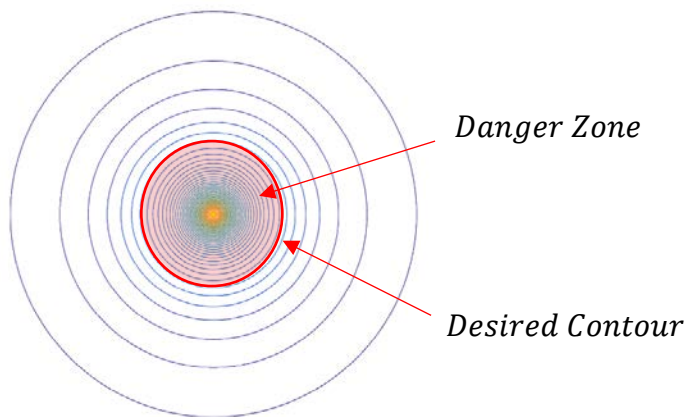
Figure 1: Desired or reference contour to be found by UAS swarm.

Much has been done in the area of radiation detection using multicopter UAS. In [6] a remote gamma ray imaging system was mounted on a multirotor drone. Citing the issue of workers accumulating too much radiation during a survey, they use the drone with onboard gamma ray camera to detect different sources of radiation. They used this drone to measure sources of radiation near the Fukushima Daiichi Nuclear Power Station. The drone uses an onboard computer to gather data through the gamma ray and optical camera via USB 3.0. The radiation detector uses less than 5 watts of power which is ideal since power usage is often critical component on a remote sensing platform. This method relies on the overlay of the gamma ray camera on to the optical

www.manaraa.com

camera in conjunction with the GPS sensor locating the source. This method is good for monitoring known locations of sources of radiation rather than trying to find unknown source locations.

A Number of methods have been developed for locating radiation sources with a single UAS. One of which is a recursive Bayesian estimation approach used by [7], for locating the source of a known model of radiation. This method uses a single UAS to measure the strength of a source via an onboard radiation sensor. The method uses an initial guess to predict the state, the location of the source in relation to the UAS, then uses sensor measurements obtained from the sensor to correct that initial guess and continue the prediction. This method is useful because it can locate the source using current and previous measurements gathered from the sensor even though the radiation sensor in the case is operating essentially as a distance sensor. Brewer et al successfully implemented this method in experimentally locate a source of radiation [7]. A downside of this method is its diversion from the true state when measurements are noisy or the process is not modeled correctly.

Formation control has been studied extensively in [9-14]. Many of these works are based on circular formation of agents with an overall swarm heading angle determined by appropriate control schemes providing trajectories of each UAS. Arranz et al. has done work related to the formation control of UAS swarm under finite communication range [13]. This can be important due to typical range restrictions of most multicopter UAS. Arranz et al claims that this is applicable for situations in which "agents should perform collaborative tasks requiring the formation to navigate towards a priori unknown direction." This is particularly pertinent for source seeking and contour mapping since prior knowledge of the source is not known before the UAS swarm starts to perform its task.

Different algorithms for determining the locations of radiation sources using simultaneous measurements taken from UAS swarm in formation have been studied including gradient-based methods. Generally, to accomplish contour mapping, the swarm of UAS with on board sensors uses gradient estimation to determine the steepest gradient which governs a bulk heading vector for the swarm to follow [7, 15, 16] . Ogren et al. have developed an algorithm for gradient detection where a networked group of UAS each with a single sensor adaptively determines the gradient. Source seeking behavior can be accomplished by directing the swarm in the direction of most increasing gradient. Han J. et al. shows both source seeking and contour mapping methods using a UAS [16]. They first start with a source seeking strategy then augment the heading of the swarm to move tangentially to the source once the reference contour is reached.

However, conventional algorithms are effective only in a specific set of circumstances with particular initial conditions. Also, implementation of actual UAS in a swarm formation was not validated in experimental test bed in the context of radiation source seeking and contour mapping.

The main contribution of this work is to develop computer simulation platform for UAS swarm based source localization and contour mapping technique including UAS dynamics as well as its flight simulation in realistically simulated radiation field for the UAS swarm to map. Also, a novel algorithm for the heading angle is presented to provide near minimum flight trajectories for a UAS swarm contour mapping. The computer simulation results of source seeking and contour mapping are validated with two types of UAS, small and medium sized multicopters, in the indoor flight testbed located in UNLV.

The thesis is organized by 6 chapters. Chapter 1 is an introduction to radiative sources practical uses of UAS, UAS swarms. Chapter 2 discusses the uses of radiation sensors onboard the UAS, plug and play functionality of those sensors, and a simplified radiation model used for

4

simulations. Chapter 3 describes the algorithms used for gradient estimation, contour mapping and the feedback controller used to guide the swarm. Chapter 4 discusses the computer simulation platform for inclusion of UAS dynamics and simulations within a more realistic radiation field model. Chapter 5 shows the experimental setup used including the indoor flight testbed with motion capture, ROS, and analogs to radiation sources used in the experiments. Chapter 6 discusses the results of both contour mapping and source seeking UAS swarm behavior.

Chapter 2: UAS Based Radiation Measurement

2.1 Radiation Source and Contour Mapping

One of great potential applications of UAS can be found in remote radiation mapping and localization of radiation sources. As shown in Figure 1, for an ideal isometric point source of radiation, the inverse square law "$\frac{1}{r^2}$" describes intensity falloff that a sensor would experience with an increased distance away from the source.
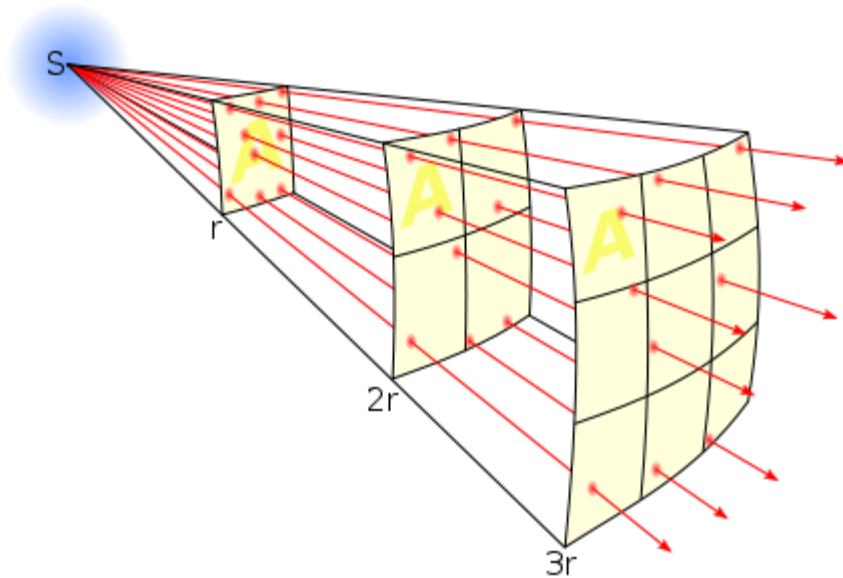
Figure 2: Inverse Square Law by Borb (https://en.wikipedia.org/wiki/Inverse-square_law#/media/File:Inverse_square_law.svg, Picture is licensed under Creative Commons BY 2.0)

The ability to locate a source of radiation following the $\frac{1}{r^2}$ model using a UAS swarm is valuable in many cases but it does not give an operator an idea of the area of danger due to the radiative source, only the central location. To be able to find the safe area away from the source it is necessary to find a desired contour or particular sensor strength of the scalar field generated

6

by a $\frac{1}{r^2}$ source. This is shown in Error! Reference source not found. where the source is located at (50,50).
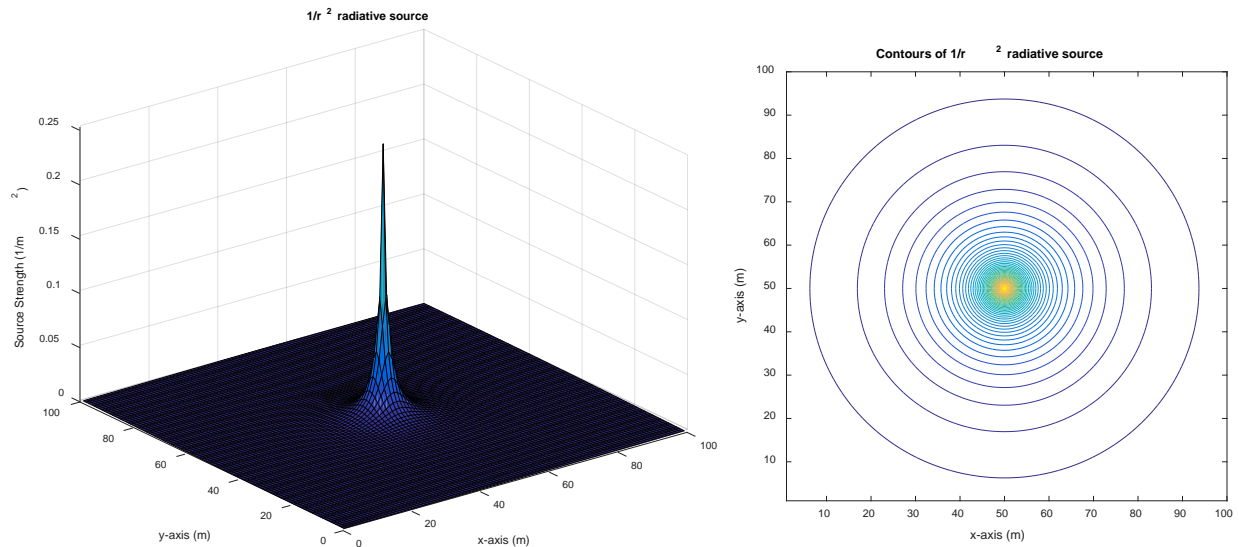
Figure 3: Intensity of a source located at (50,50) and contours generated by that source.

Contour mapping [16] is the idea to try to find "contour" of the source at a certain strength. This strength level is whatever is desired when setting a reference value but could be something as simple as a level of radiation that is safe for a human for a certain amount of time. A UAS swarm can be used to find this contour faster than is possible by a single UAS or manually first responder and provide a safe boundary for any disaster situation where first responders need to know what area or zone is unsafe to enter.

2.2 Radiation Sensor

The choice of radiation detector is important when the sensor is considered for a UAS platform. Weight is the main factor since the flying efficiency of a quadrotor is drastically reduced with an increase in weight. Some radiation detectors also need active cooling which isn't easily

7

feasible on a UAS. For these reasons, the Kromek USB-powered CZT detector was chosen for each UAS platform. CZT detectors are semiconductors that convert x-ray or gamma-ray photons into charger carriers. The detector is capable of high-resolution ambient temperature gamma-ray spectroscopy. The detector module itself weights 49.2 grams, measures 2.5 x 2.5 x 6.1 cm and uses a $1cm^3$ cadmium zinc telluride crystal. The sensor has an energy detection range from $30KeV$ to $3.0MeV$ with an energy resolution of less than 2%. The detector interfaces directly through USB to a computer onboard the UAS.

Figure 4: Kromek cadmium zinc telluride (CZT) based detector.

The gamma ray spectrum is generated from the counts obtained by the detector and Mariscotti's technique is used for the identification of peaks[17]. An example of this is shown in **Figure 5** with readings from Cobalt 60 and Cesium 137.

8
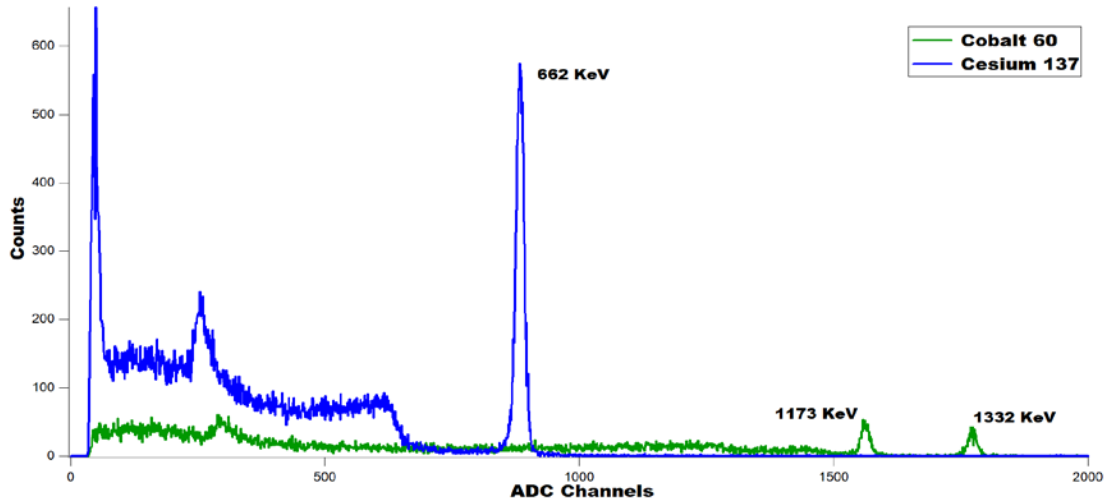
Figure 5: Gamma ray Spectrum generated by Kromek detector.

2.2 Plug-and-Play Functionality

To facilitate ease in implementation of the desired sensors, plug-and-play functionality was developed for each sensor. The sensors are all interfaced through USB and can be "hot swapped" without having to shut down power to the entire UAS. There is an onboard powered USB hub that connects to an onboard computer used to interface with all the sensors and any communication methods (radios, WIFI, etc.) used to relay information to a ground station operator. **Figure 6** shows a gas sensor and radiation sensor that are both interfaced through USB.
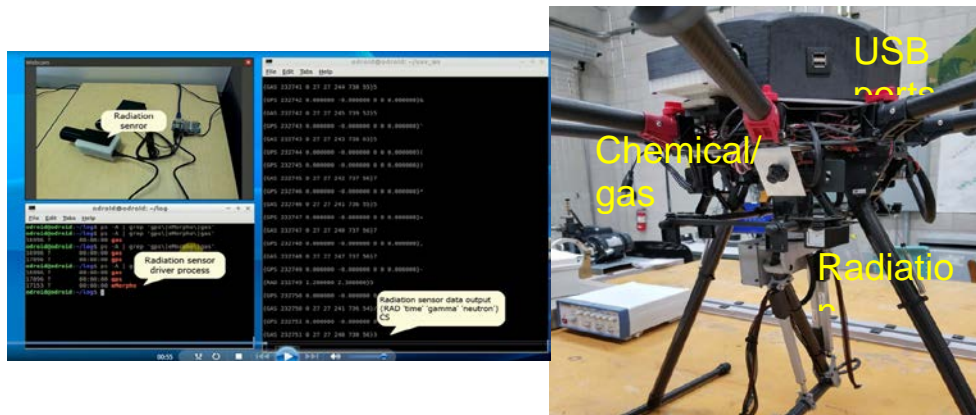
2.3 Simulated Radiation Field

For initial simulations, a $1/R^2$ model is used for the radiative sources with R being the distance away from the source. From the scalar field generated by the model, a vector field is created to visualize the gradient at any position produced by the source. These fields are shown in **Figure 7.**
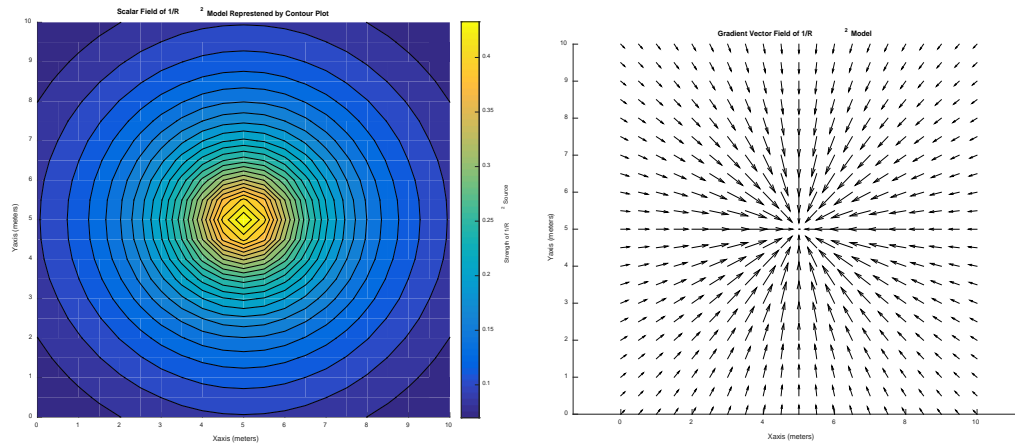
Figure 7: Simplified radiative source model used for initial simulations.

Chapter 3: Algorithims for Gradient Estimation and Contour Mapping

3.1 Gradient Estimation

This method of gradient estimation uses the average of sensor measurements over a closed region.

The average of the scalar field is taken over a disk centered at c in R^2 with radius r.
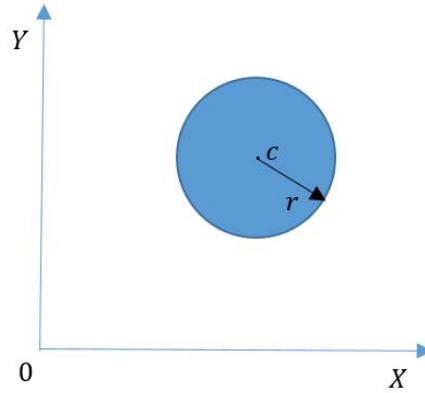
Figure 8: Disc located in a scalar field of sensor measurements.

The average of scalar field would be represented by:

$$T_{ave}(c) = \frac{\int_\Omega T(x)\,dx}{\pi r^2} \tag{1}$$

Where Ω is the area of the disc and T(x) is the strength of the sensor reading at any point x on that disc. The ultimate goal is to figure out which way to move the center of the disk in order to increase the average of the readings from Eq.1 . Uryasev [18] shows that using the average measurement, the gradient can be written as :

$$\nabla_c T_{ave}(c) = \frac{\nabla_c \int_\Omega T(x)\,dx}{\pi r^2} = \frac{1}{\pi r^3} \int_{\delta\Omega} T(x)\,(x - c)dS \tag{2}$$

11

Where $\delta\Omega$ is the boundary of Ω. Ogren, P [19] shows that with finite number N of sensor measurements T_n at points $x_i, i = 1, ..., N$; using the assumption that the N measurements that are taken are uniformly distributed over the circle, and using the composite trapezoidal rule, we obtain:

$$\frac{1}{\pi r^3} \int_{\delta\Omega} T(x)\,(x - c)dS \approx \frac{1}{\pi r^3} \sum_{i=1}^{N} T_n(p_i + c)p_i \Delta s \tag{3}$$

Where $p = x - r,\ p_i = x_i - c$ and $\Delta s = 2\pi r / N$. This is the general case, and if changing the coordinates such that the origin coincides with the center of the disk the equation becomes:

$$\boldsymbol{\nabla_c T_{ave}(c)} \approx \frac{2}{Nr^2} \sum_{i=1}^{N} T_n(\boldsymbol{p_i})\boldsymbol{p_i}\Delta s \tag{4}$$

In this case the position of each UAS and its measurement will approximate integral the gradient since only a finite amount of UAS and therefore sensor measurements can be used. The swarm formation used has $N = 3$ UAS distributed equally around a circle.
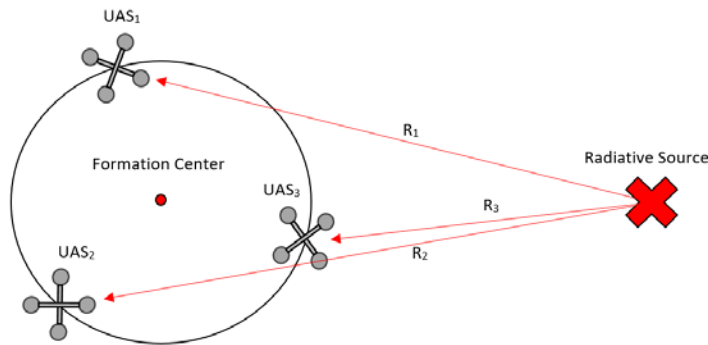
Figure 9: The sensor strength corresponding to each UAS' measurement from the radiative source follows the $Tn\,(i) = \text{pwr}/Ri^2$ model.

12

Using **Eq. 4** an estimated horizontal and vertical component of increasing gradient can be determined. The formation center can then be moved in relation to the now known estimated direction of increasing gradient for source seeking behavior for the swarm.

It is possible to use any desired number of UAS within the swarm. With any number of UAS in the swarm, the gradient estimation necessitates the UAS be evenly distributed around a circle for the algorithm to operate the most accurately.

3.2 Error in Gradient Estimation Algorithm

There is an error inherent within the algorithm's estimation of heading within a $1/r^2$ field. A relatively small change in distance can have a huge effect on the strength of the source for each UAS. If the radiative source to be measured behaved more linearly with distance there would not be as big of an error with respect to estimated source direction. This error along with a few examples of the position of the swarm vs. the position of the source is shown below in **Figure 10.**
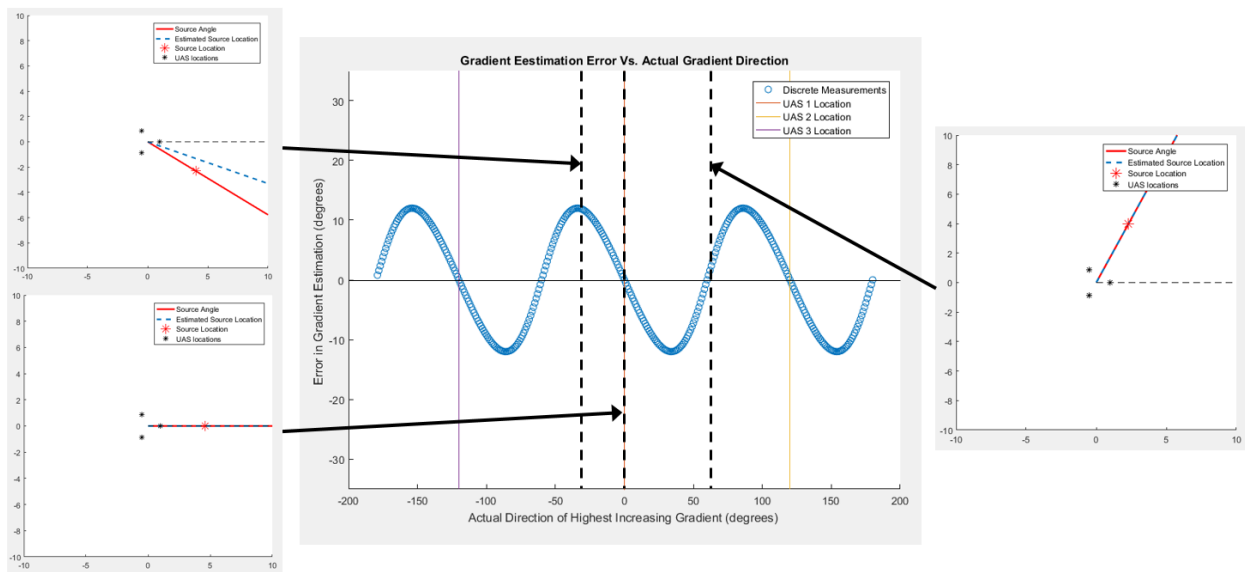
Figure 10: Error of gradient estimation algorithm, Swarm radius = 1m, Source distance = 5m.

The error for the estimated angle of the source increases when $\frac{Swarm\ Radius}{Source\ Distance} \rightarrow 1$. When the source distance is far away, as shown on the left side of **Figure 11**, there is +-4 degree error which is small. When the source distance is very close to the nearest UAS, there is a +-30 degree error shown on the right side of **Figure 11.**
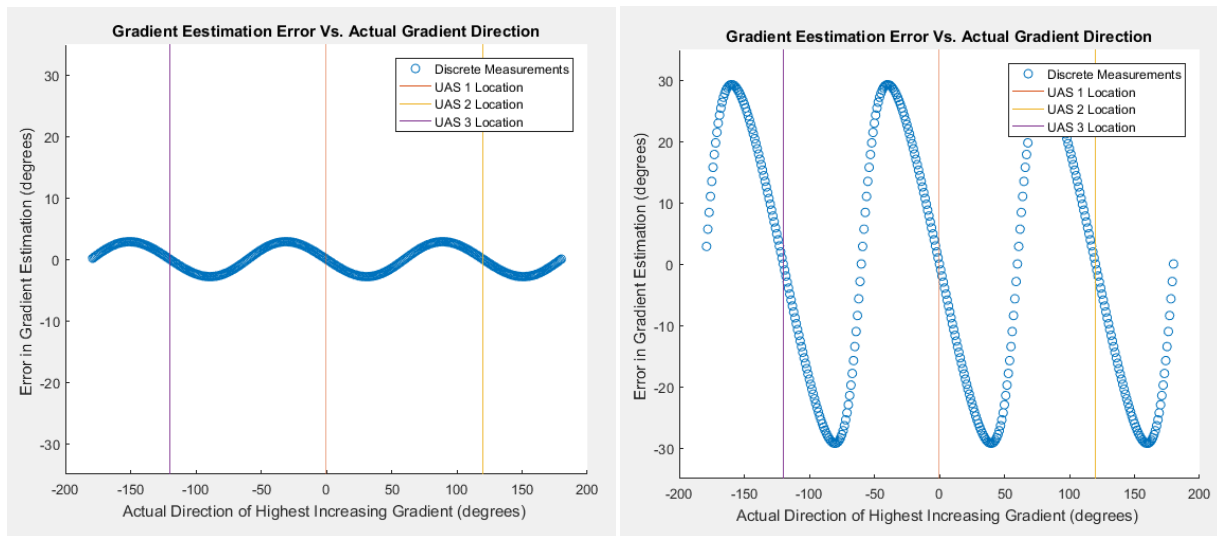
Figure 11:(left) Swarm Radius= 1m, Source Distance = 20m. (right) Swarm Radius = 5m, Source Distance = 6m.

A GUI was created within Matlab to show the relationship between these two variables more easily. There is also the ability to switch from 3 to 5 UAS to show the difference in expected error for the gradient estimation algorithm depending on the number of UAS in the swarm.
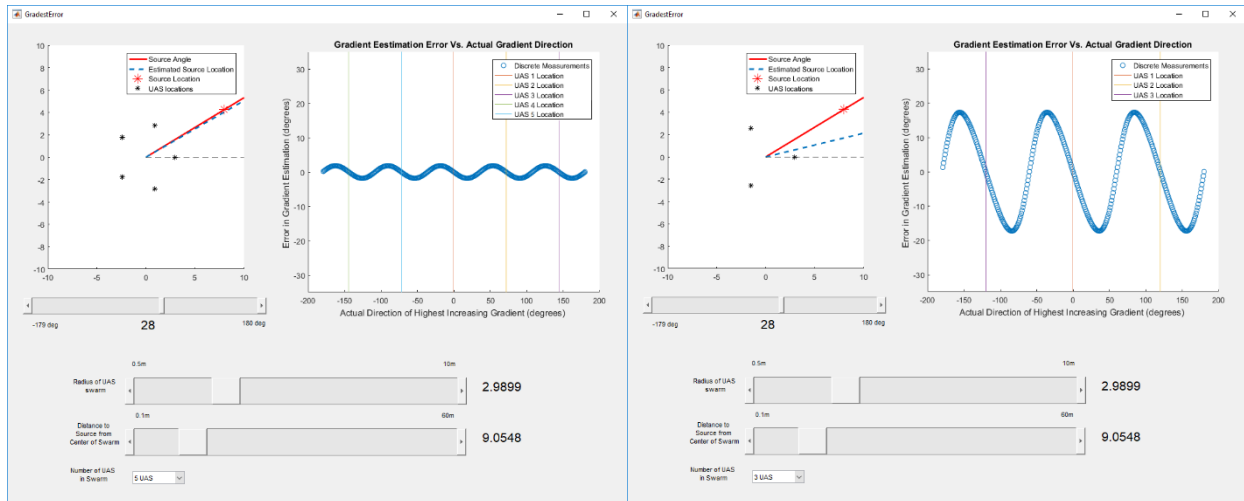
Figure 12: (left) 5 Agent UAS Swarm (right) 3 Agent UAS Swarm

3.3 Swarm Heading Determination for Contour Mapping

Source seeking behavior is demonstrated when the swarm heads straight toward the source. While this can be helpful for certain tasks, it doesn't help with finding a perimeter of safety in the case of a disaster situation. Contour mapping is used to find the desired a contour of a predetermined strength. If traveling perpendicular to the estimated gradient angle then the swarm will follow the contour of the source at whatever strength it is currently measuring, which is why $\frac{\pi}{2}$ is subtracted from the estimated source angle in figure **Figure 13** however, there needs to be another contribution, the "control angle" Φ, to the overall swarm heading angle to bring it closer or father away from the source depending on where the swarm is in comparison to the desired contour.

15

$$\text{Swarm Heading Angle} = \Psi = \theta_H - \frac{\pi}{2} + \Phi$$

θ_H	Estimated gradient angle meassured w.r.t. x axis
Φ	Control angle
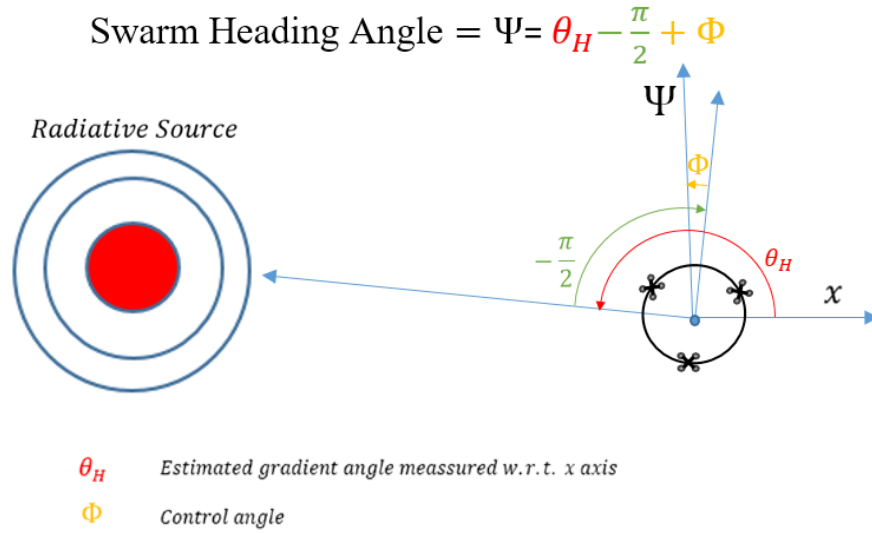
Figure 13: Swarm heading angle components.

3.3.1 PID Control of Heading Angle

The estimated gradient angle is based on the vector field for the source while the control angle is based on the average strength measurements from the UAS swarm. To steer the bulk heading of the swarm toward and then along the desired contour a PID controller is implemented. **Figure 14** shows the difference in the heading angle of the swarm depending on the distance of the control angle. If the control angle is zero the swarm will travel perpendicular to the estimated direction of the source. If the control angle is positive the swarm will travel more towards the source and conversely, if the control angle is negative the swarm will travel away from the source.
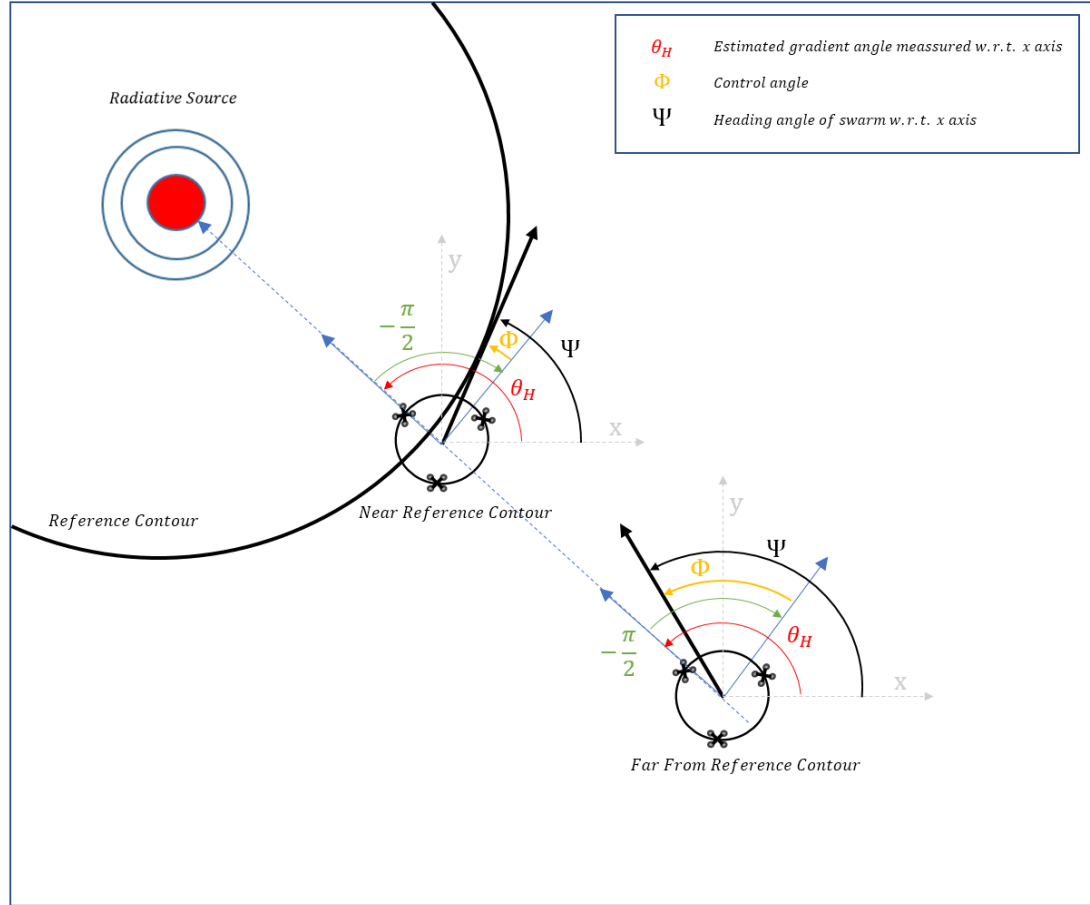
Figure 14: Shows the change in size of control angle Φ depending on the swarm's distance away from the desired reference contour.

Error for the heading angle controller is defined as:

$$E_s = Error = S_r - S_m \qquad (5)$$

$$S_r = Reference\ Mean\ Sensor\ Measurement$$

$$S_m = Measured\ Mean\ Sensor\ Measurement$$

The average sensor measurement of the radiative field is S_m is subtracted from the desired,

or reference, sensor measurement. This is then used in a conventional PID equation:

17

$$K_p E_s + K_i \int_{t_0}^{t} E_s dt + K_d \frac{E_s}{dt} \tag{6}$$

A mathematical construct is used to aid in determining the control angle. Using a right triangle with the sides R_1 and R_2. R_1 is a constant that is small enough for R_2 to have an effect when the contributions from error are relatively small when considering a $\frac{1}{R^2}$ type source.
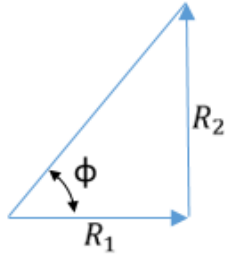
$$R_1 = constant$$

$$R_2 = K_p E_s + K_i \int_{t_0}^{t} E_s dt + K_d \frac{E_s}{dt} \tag{7}$$

$$\phi = \tan^{-1}(\frac{R_2}{R_1})$$

As shown in **Figure 14,** If the swarm is close to the reference contour then the control angle is small because there is relatively small error contribution to R_2. If the swarm is far from the reference contour the swarm's control angle is bigger because of a larger contribution through the PID control to R_2. Equation (**7** needs to be discretized to be used in the simulation and to be implemented on the computers onboard the UAS themselves.

$$R_{2_k} = K_p E_s + K_i \sum_{i=1}^{k} E_s(t_k) + K_d \frac{E_{s(t_k)} - E_{s(t_k-1)}}{\Delta t} \tag{8}$$

3.3.2 Anti-windup

Integrator Windup happens when "actuator effort" is saturated and there is still an increasing integration contribution in the PID control. This causes an overshoot of the desired setpoint (or contour). Actuator effort in this system is defined by how close the absolute value of the control angle is to $\pi/2$. **Figure 15** shows the difference in actuator control effort between a large and small control angle. As the swarm travels relatively straight towards the contour the control effort is nearly maximized, or saturated, and if a substantial amount of integration of error happens during this time there will be overshoot of that contour. If that integration of error is reduced while the swarm is heading toward the desired contour, once it reaches the contour the swarm should be able to follow it much better when it initially reaches the contour.
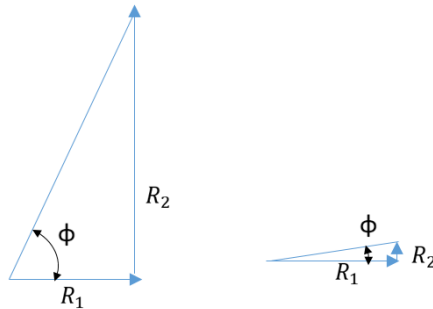
Figure 15: Control angle differences based on error contribution of PID through R_2.

To reduce the integration when the control angle is nearly maximum, **eq. (9)** is used for R_2. **Equation (9)** shows the integrated term but instead of linearly accumulating on every iteration, it is multiplied by the cosine of the previous control angle. If the control angle is big, meaning the control effort is near saturation, the contribution to the integrated error will be minimal. This method is called Anti-Windup and when it is incorporated within the mapping algorithm there is a marked decreased in the amount of overshoot of the desired contour.

$$R_{2_k} = K_p E_s + K_i \sum_{i=1}^{k} (E_s(t_k) * \cos(\phi_{t_{k}-1})) + K_d \frac{E_{s(t_k)} - E_{s(t_k-1)}}{\Delta t} \qquad (9)$$

When running the simulation with anti-windup, Figure 16 shows that there is a more gradual accumulation of error which allows a minimization of overshoot of the desired contour.
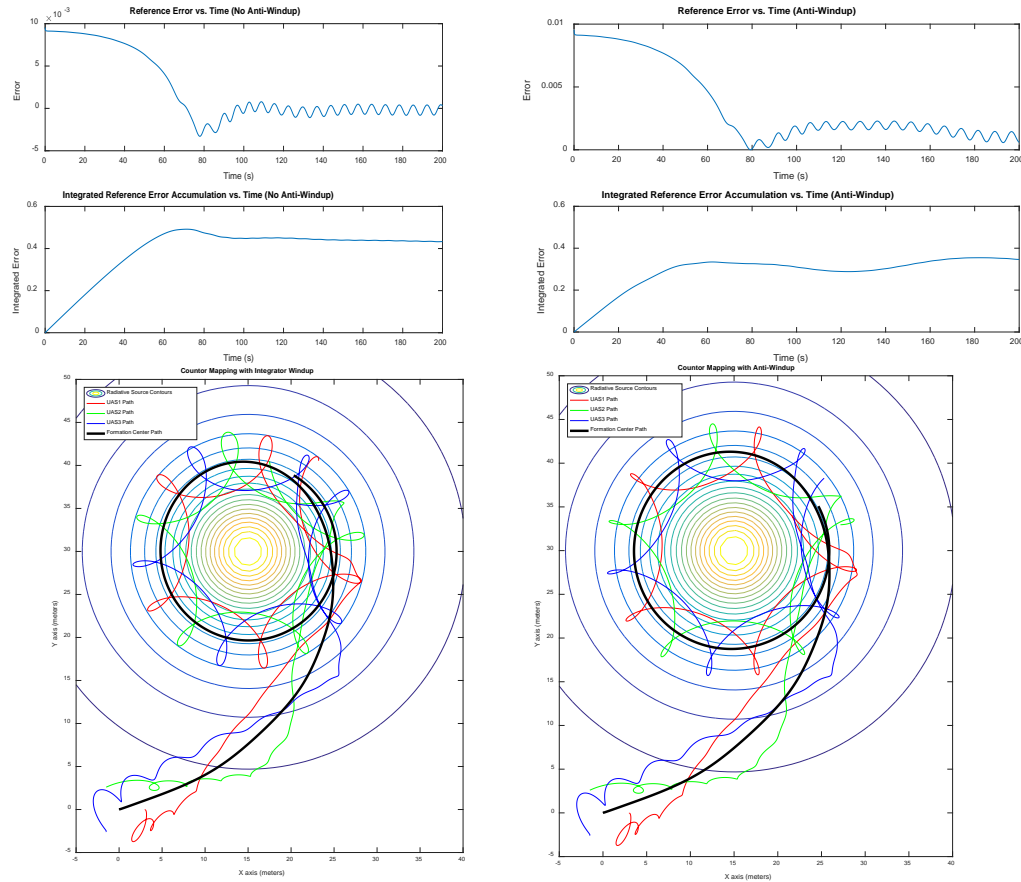
Figure 16: On the left is the contour mapping algorithm without the use of anti-windup. The error accumulates much faster and causes overshoot of the desired contour. The right shows the system with anti-windup which prevents the "I" term from having too big of an effect while the system is trying to get closer to the reference contour.

20

3.4 Swarm Rotation and Adaptive Rotation Rate

When there is no spinning of the swarm there is evidence of the gradient estimation errors like those shown in Error! Reference source not found. when attempting the contour mapping. When there are three UAS agents in the swarm the error in the gradient estimation algorithm, when attempting to map a circular contour, will manifest in the trajectory as a rounded triangle. To counter act this, spinning is introduced to improve the accuracy of the followed contour. When the swarm is spinning, the error estimation is still present but is at such a high frequency when compared to a non-spinning swarm that the effect of the error is negligible on the overall formation path. **Figure 17** shows the difference between a non spinning and spinning UAS swarm when trying to implement contour mapping.
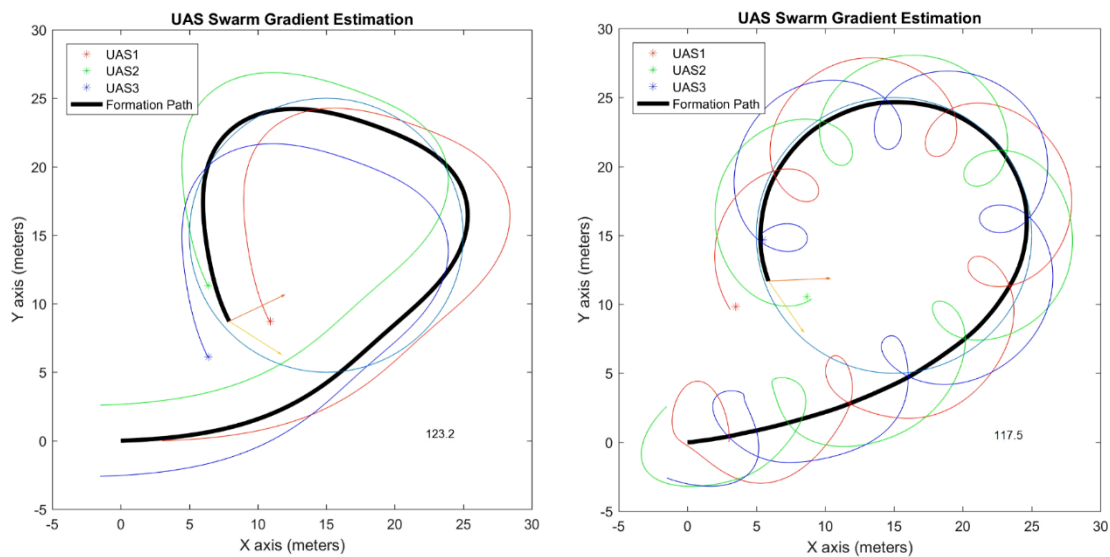
Figure 17:A spinning formation is used to counteract 'artifacts' shown on the right in the contour mapping due to the error inherent in the gradient estimation algorithm. When spinning, a much more precise boundary of the source can be achieved.
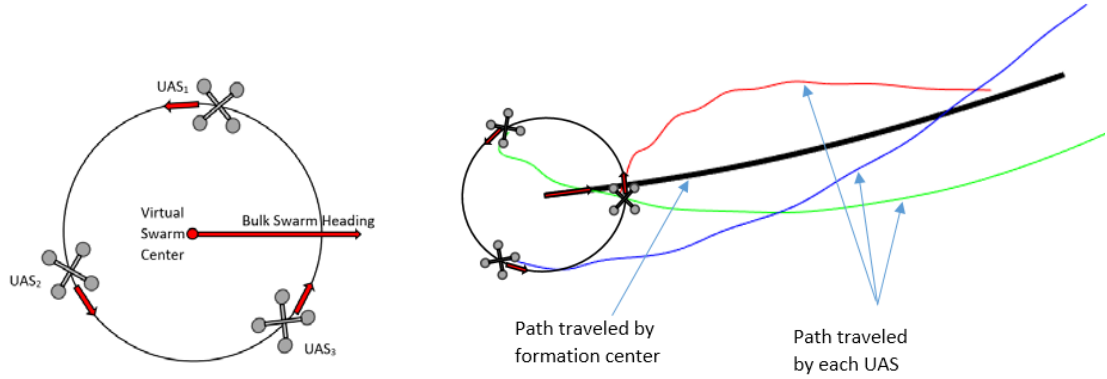
Figure 18: UAS swarm spins around virtual center position to help counter act error from gradient estimation algorithm

Spinning of the swarm can cause an increase in path length so care was taken to decide the rotational speed of the UAS swarm. **Figure 18** shows the UAS swarm formation. The swarm circles around a virtual center while that center travels in the direction dictated by the swarm heading algorithm. Depending on the swarm rotation rate a large increase in path length can occur over the duration of the flight. There is a nearly negligible difference in path length if the swarm spins clockwise or counter clockwise. Simulations for rotation rates at $0, \pm0.075, \pm0.1, \pm0.2$, and ±0.3 rad/s were ran for 150 seconds and the average of the path lengths for each UAS in the swarm was plotted vs the rotation rate in **Figure 19**.
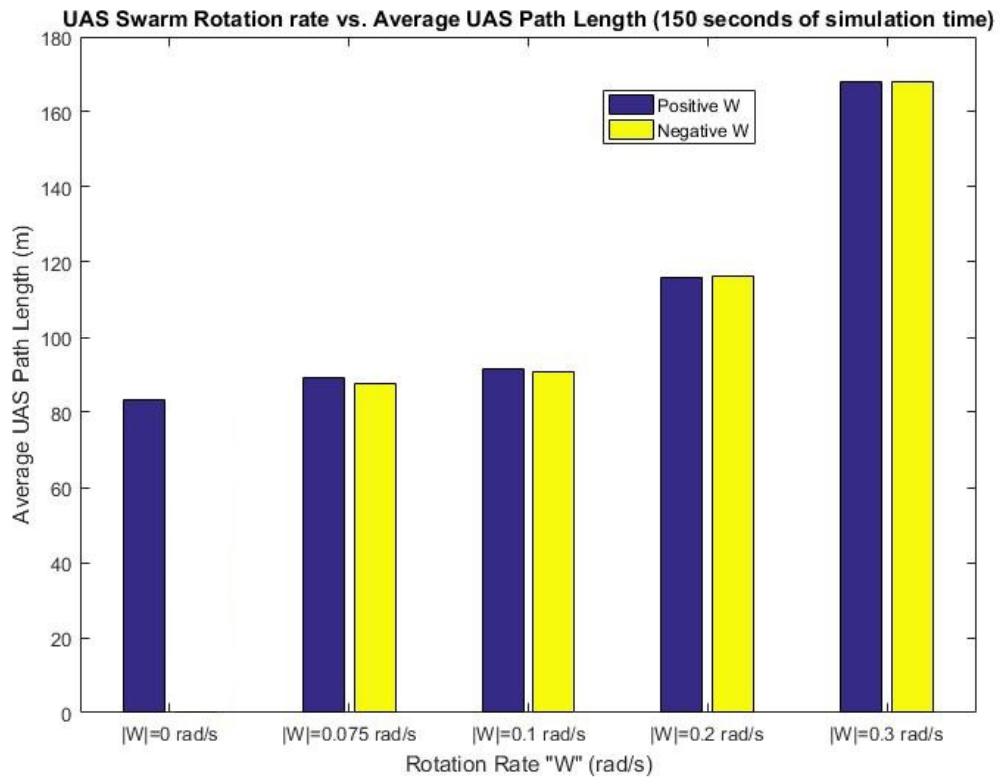
Figure 19: Rotation rate can have a huge impact on the distance that each UAS is required to travel. Reducing the spin rate will reduce the path length and allow longer mapping trajectories but at the cost of mapping accuracy.

Reducing the rotation reduces the total distance that each UAS in the swarm will have to travel, extending the size of contour that the swarm could map, but at the expense of mapping accuracy. Five rotations of the UAS swarm per circumnavigation of a circular contour, at whatever contour radius, was chosen for a balance between mapping accuracy and overall mapping time. The equation used to determine reference swarm rotation rate is shown in **Figure 20.**

23
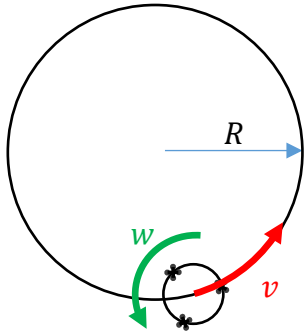
$$\frac{circumference}{v} = time \ (\ per \ contour \ circumnavigation\ )$$

$$\frac{Swarm \ Rotations_{desired}}{time} = w \ (desired \ warm \ rotation \ rate)$$

$$\frac{5(rot._{des.})*2\pi}{\frac{2\pi R}{0.5\frac{m}{s}}} = w$$

Figure 20: The desired rotation rate is a function of the radius of curvature that the UAS swarm is traveling, the speed of the swarm, and the number of rotations desired per circumnavigation of the contour.

Using the discrete positions of the center of the UAS swarm, it is possible to determine the radius of curvature of the path that the swarm is on and apply that to the equation in **Figure 20** to adapt the rotation of the swarm as needed. A least squares fit to a circle was used to find the radius of curvature using a buffer of the last traveled coordinates of the swarm [20][21]. **Figure 21** shows the effect of the adapted rotation rate on the swarm path. This allows for minimal rotation when the UAS swarm is far from the contour and increase the rotation rate when we are near the desired contour. The rotation rate control is saturated with a lower bound of 0.05 rad/s and an upper bound of 0.3rad/s. There is a big spike in the radius of curvature for the swarm when the simulation is started dude to the nearly linear path that the swarm follows.

24
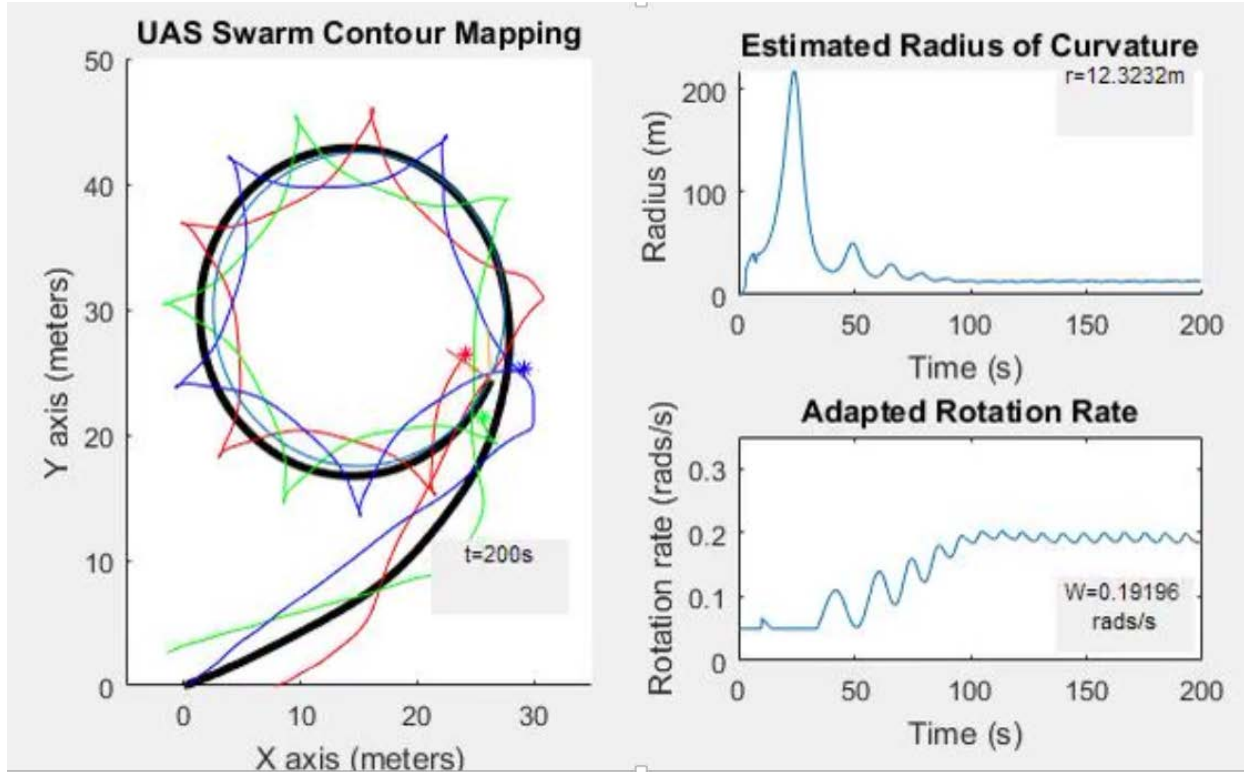
Figure 21: As the estimated radius of curvature approaches the target contour located at 10m the rotation rate converges toward the desired 0.25 rad/s

Chapter 4: Computer Simulation Platform

In order to verify the gradient estimation, source seeking, and contour mapping algorithms, a simulation platform was developed. The simulation results are used to inform further decisions on what needs to be changed and tuned before implementation within a physical UAS swarm.

4.1 UAS Dynamics

Previous simulations of contour mapping and source location generally do not consider UAS dynamics. **Figure 22** shows the difference between the inclusion and non-inclusion of UAS dynamics on the trajectory that the swarm is able to follow. If dynamics are not a concern it is fastest to head straight to the source until the reference contour is reached then travel perpendicular to the direction of the source which map the contour. When reaching the contour in the kinematic simulation, there is an unrealistic trajectory for a real UAS to follow. There is a sharp right turn that would not be able to be followed when the swarm has a constant velocity. When incorporating dynamics within the simulation a more indirect but realistic trajectory is generated by the heading angle controller illustrated in **Figure 14**.
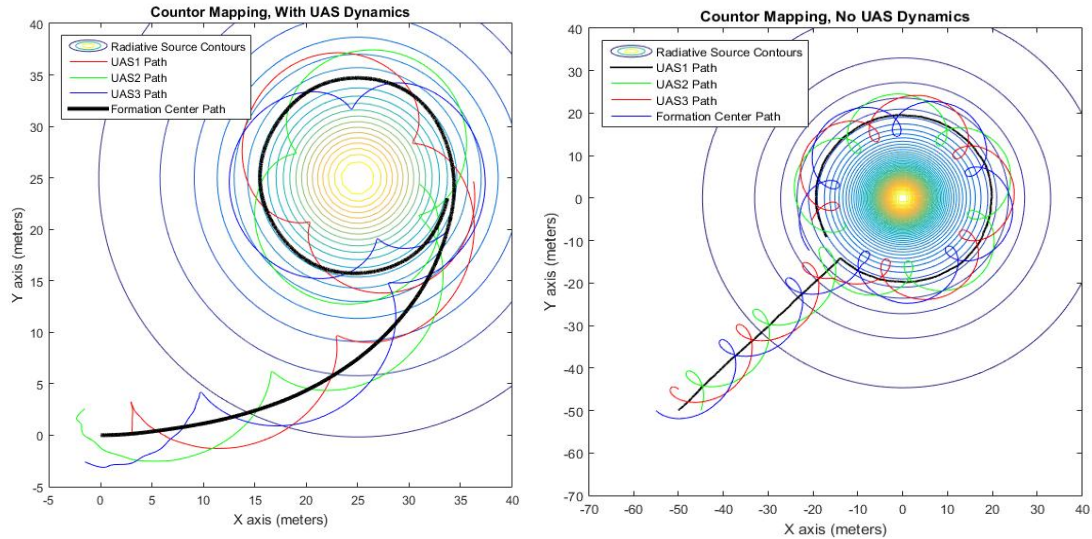
Figure 22: Double Integrator system incorporated in Simulink to approximate UAS dynamics. This provides a much more realistic simulation instead of the right angle turns when only kinematics are considered.

In order to determine the parameters for the simplified UAS dynamics model, a Crazyflie2.0 was flown within the motion capture flight volume in order to determine its approximate acceleration and maximum velocity. These parameters were applied to the Simulink model. A simplified version of the Simulink model is shown as a flow diagram in **Figure 23** . The simulation is composed of 4 main parts: Formation Control, Quadrotor model, Gradient estimation and Heading Control. Starting with the formation of the UAS in the swarm, there is a reference position that is generated that is fed to the PID controller of each UAS agent. Using those reference positions each agent try to reach its reference position. Next, the gradient detection algorithm

27

occurs and that is fed into the heading control of the whole swarm so new reference positions can be generated for the UAS swarm so that the swarm can travel in the new desired direction.
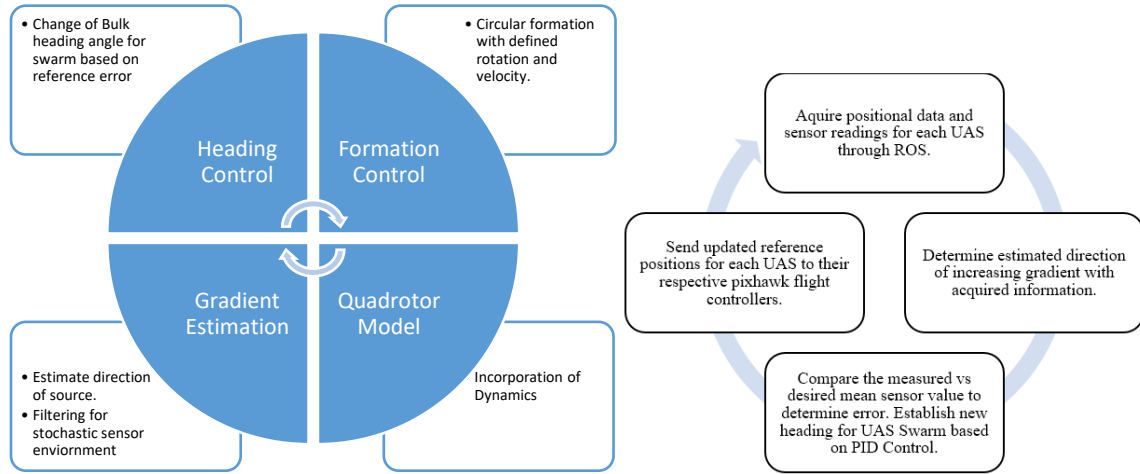
Figure 23: Simplified flow diagram of Simulink model.

4.2 Filtering

A stochastic model of radiation was used to increase the realism of the simulation. For every sensor reading that a UAS had, random artificial noise was introduced to the radius component of the $1/R^2$ model, an example of which is shown:

$$Sensor\ reading = \frac{1}{(R + noise)^2} \tag{10}$$

In the example shown in **Figure 24**, noise on the order of 0 to ±2.5 m was used which caused very erratic gradient estimation and heading generation, as expected. The constantly changing heading also caused the swarm to drastically slow down when preforming the contour mapping. To reduce this effect a moving average filter was applied to both the gradient estimation and the heading generation. This smoothed the trajectory for the swarm but understandably caused some lag for the gradient estimation since the estimated gradient angle uses many measurements

28

from the past averaged with the most current estimated direction. The lag in the source direction is easily corrected by the PID heading control.
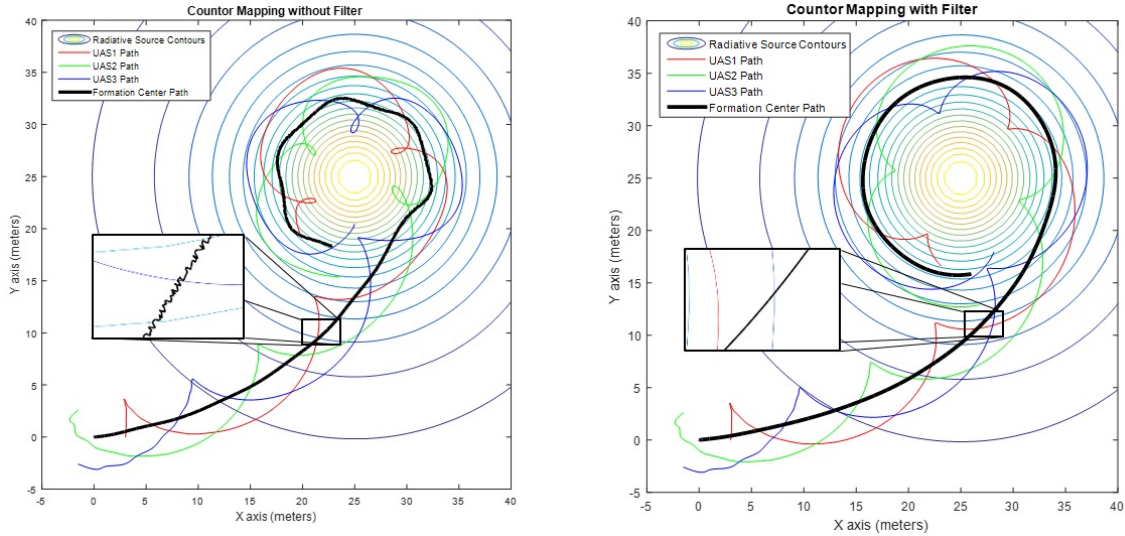
Figure 24: Stochastic sensor environment simulation with and without heading and gradient buffer. A moving average filter is employed in order reduce drastic changes in swarm heading over a short amount of time due to noise in source measurement.

4.3 Effect of control angle gain

As with any traditional PID control, there is the ability to change the heading generation control parameters to affect the trajectory taken by the Swarm. **Figure 25** shows the difference between different proportional control parameters on the on the swarm path. With a high proportional gain, the swarm will oscillate around the reference contour. When the proportional gain is lower, a more gradual route is taken toward the source till it travels perpendicular to the direction of the source on the reference contour.

29
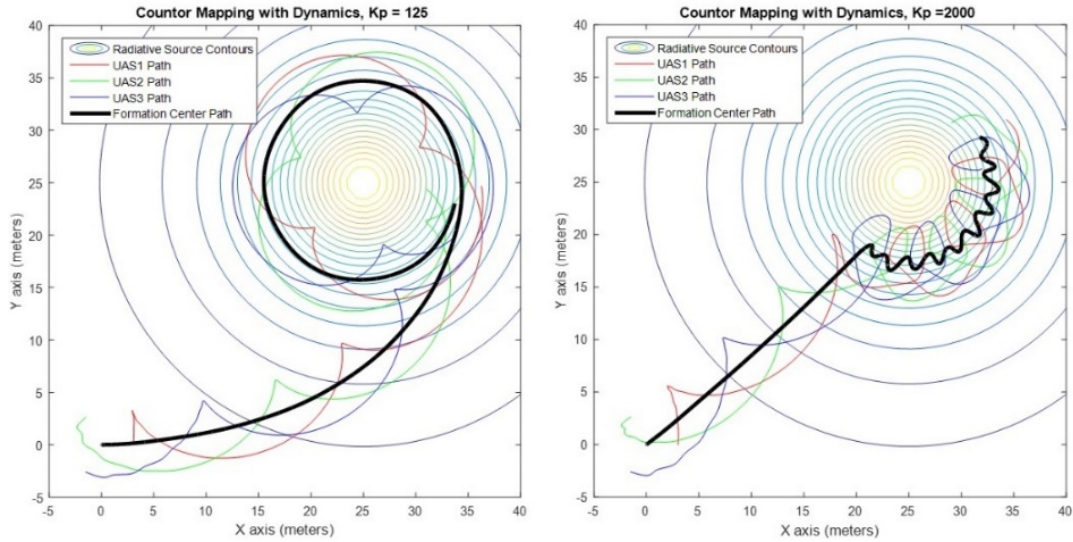
Figure 25: (left) P gain of 125 (right) P gain of 2000

4.4 Multiple sources

Mapping a continuous boundary around multiple sources is also possible without any need for alterations the swarm heading algorithms. No priori information is needed for including the strength or number of sources. Care needs to be taken though when selecting a reference mean sensor value for the UAS swarm because it is possible for the quads to map around a local maximum while missing other peaks elsewhere in the scalar field. **Figure 26** shows the swarm mapping a three-source radiative field. It is clear a local maximum that occurs close to the peak could cause the other sources in the field not to be mapped.
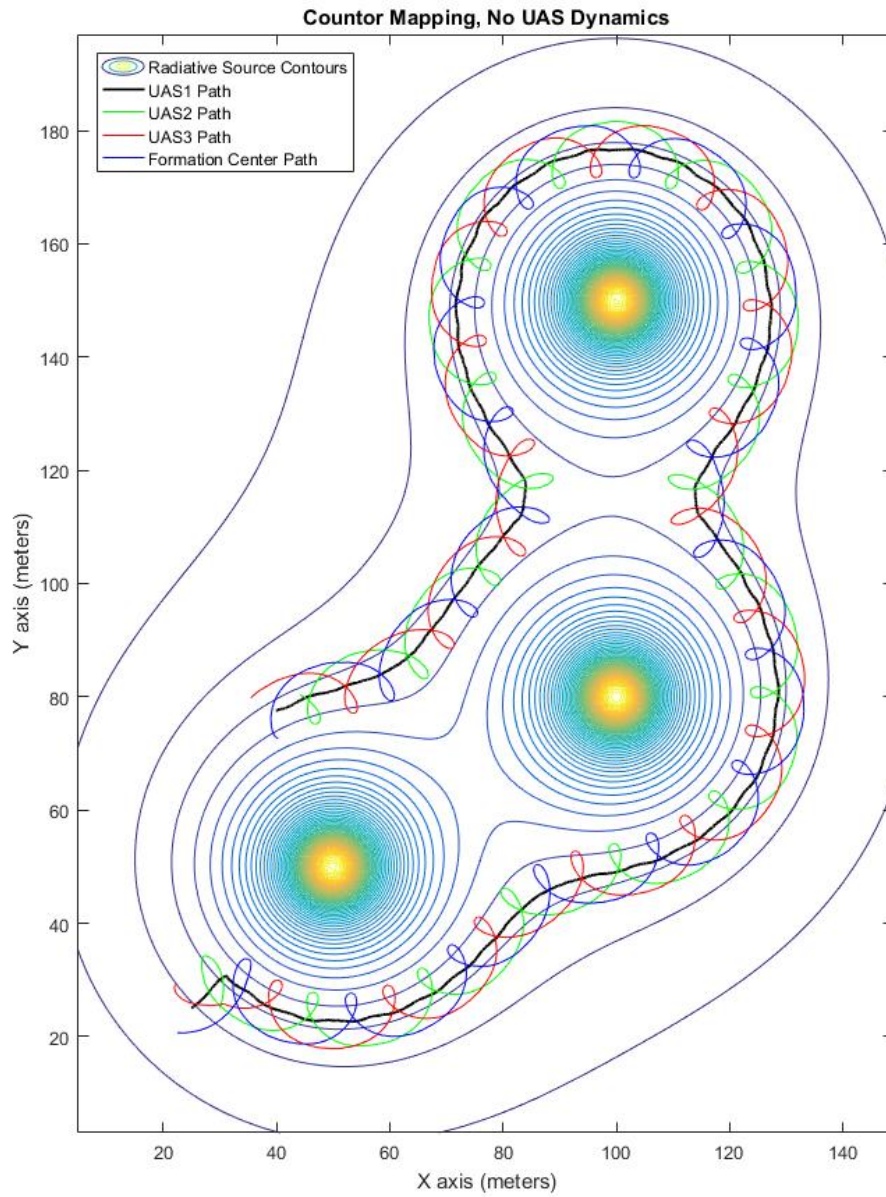
Figure 26: Simulation of the UAS swarm mapping the contour of three different sources.

4.5 Moving Source

Mapping a moving source is also possible. **Figure 27** shows a moving source traveling at 0.07 meters a second from (10,40) to (40,10). Mapping this source is possible in this particular case because the speed of the swarm is traveling at roughly seven times the speed of the source.

31

Figure 27: Contour Mapping with Moving Source

4.6 Simulation in radiation field

Monte Carlo N-Particle code (MCNP) is a general purpose code that can be used for neutron, photon and electron transport [22]. MCNP allows the simulation of a realistic radiative field and is owned by Los Alamos National Security, LLC which is the manager and operator of Los Alamos National Laboratory. The simulated radiative field 100x100x32m contained five sources of radiation ranging from 3 MeV to 6 MeV. A concrete building was also introduced into the simulation to show what would happen if a building block certain areas of radiation detection by the sensors onboard the UAS. The field generated when a height of 15m is shown in **Figure 28.**

Source Details:

- S1
  - 3 MeV @ (50,50,0.5)
- S2
  - 6 MeV @ (40,68, 0.5)
- S3
  - 3 MeV @ (5,38, 0.5)
- S4
  - 6 MeV @ (24,84, 0.5)
- S5
  - 2 MeV @ (90,60, 0.5)
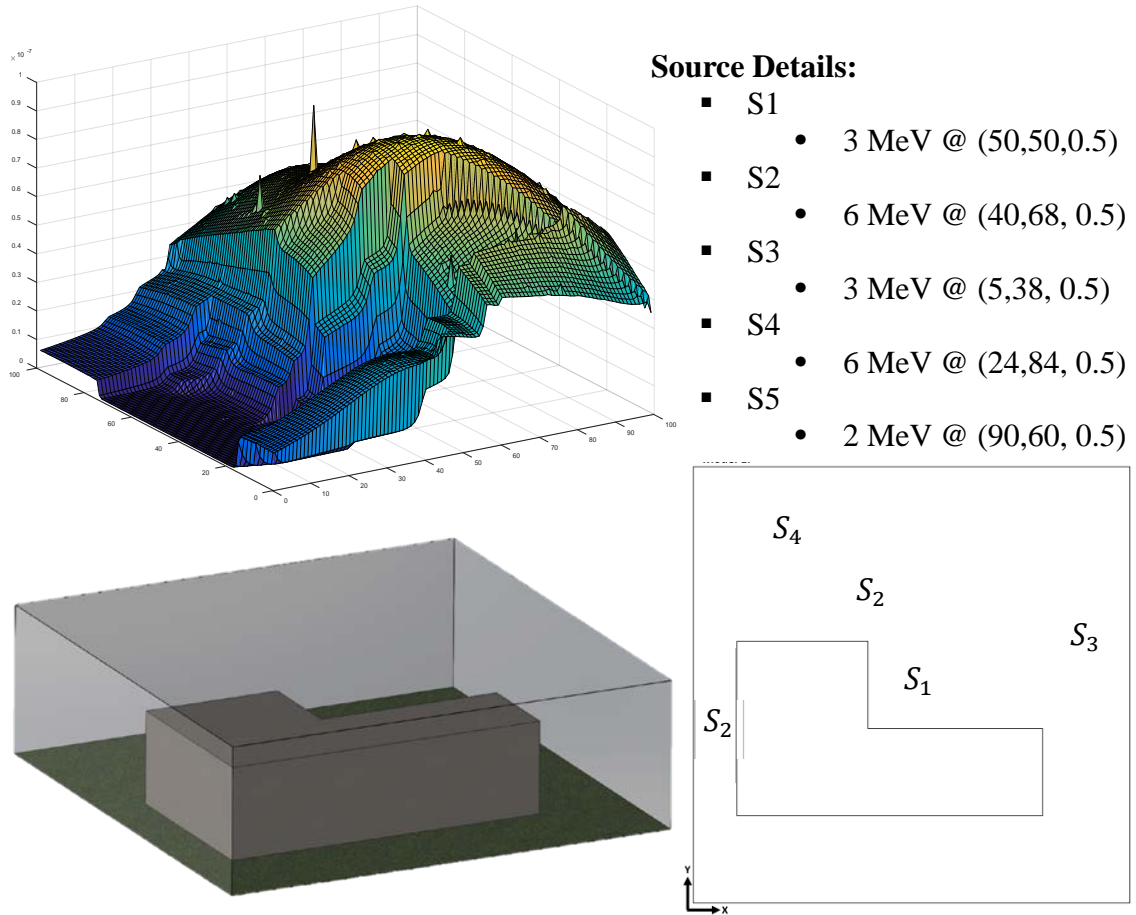
Figure 28: MCNP Radiative field generated from 5 sources and a concrete building.

The reference mean sensor value to be mapped had to be large enough so that there was a complete contour within the field generated by MCNP. The desired reference contour is shown in **Figure 29** along with the actual performance of the contour mapping algorithm overlaid onto a contour map of the radiative field. The swarm starting position within the radiation field also couldn't be started in certain positions otherwise the swarm might follow a contour which would take it out of the simulated zone. Starting the swarm at (35,35) allowed for successful mapping of the desired contour.

Reference Contour
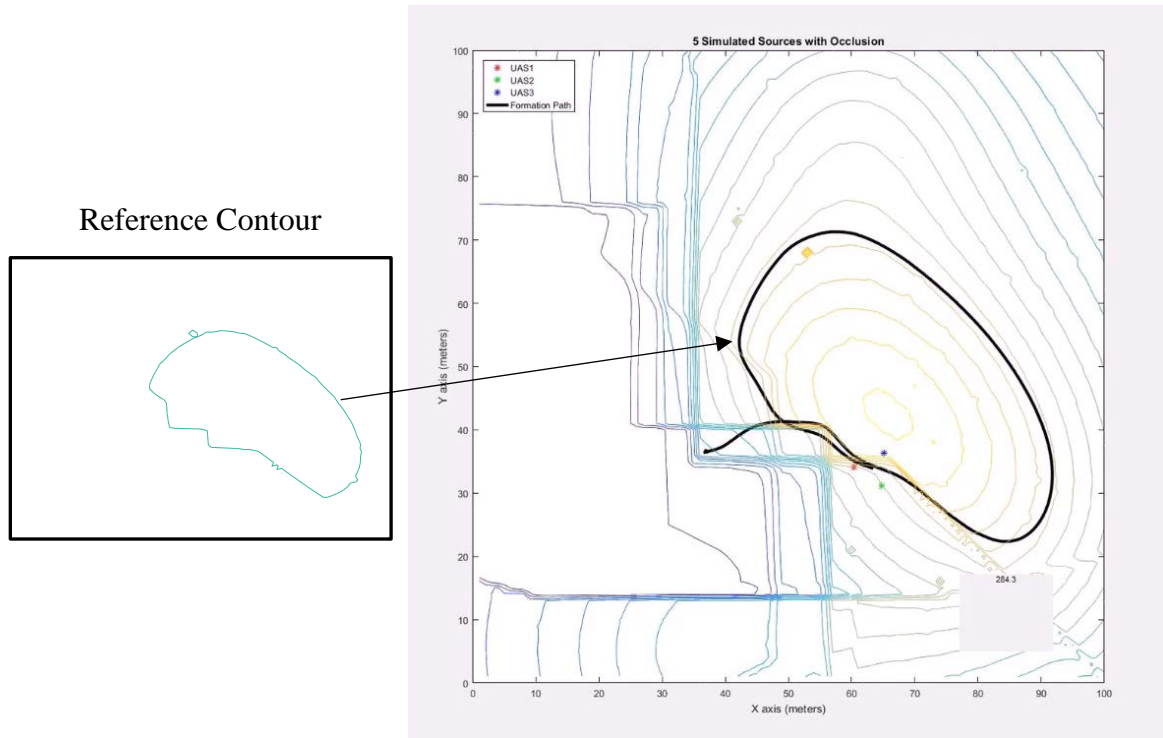
Figure 29: Contour mapping using MCNP modeled radiation field. (left) The desired contour is isolated from the field.

Chapter 5: Experimental Setup

Validation of the simulations was necessary and to do that specific UAS needed to be chosen to accomplish a given task. Limited space in the flight volume and payload capacity were the biggest constraint in choosing each UAS to preform both contour mapping and source seeking. Instead of using an actual radiation source, an isotropic light source was used as an analog to a radiation source and light sensors onboard the UAS were used to simulate a radiation detector.

5.1 UAS configurations and specifications

The Crazyflie 2.0, developed by Bitcraze, is an open source quadcopter designed to be small, lightweight, and easily modifiable. This platform was chosen due to its small size and advanced computational abilities [23]. The small size of the Crazyflie 2.0 allowed for validation of the contour mapping algorithm through experimentation inside the motion capture flight volume with a physical UAS swarm rather than simulated agents.

Crazyflie 2.0 Specifications:

- 27-gram weight
- Robot Operating System (ROS) support
- 2.4-GHz radio with 1-km LOS range
- Integrated open source flight controller
- 7 minute flight time

Figure 30: Crazyflie 2.0 with 3D printed propeller guards. The reflective markers for motion capture are placed along the propeller guard in a formation unique to each UAS.

35

The DJI Flamehwheel 450 was chosen for an experiment using real sensors due to its payload capacity while still being small enough to fly three in the given flight volume. **Figure 31** shows the Flamehwheel F450 along with the single board computer that is mounted to a 3D printed mounts under the frame.

DJI Flamehweel 450 Specifications:

- 2.5-lb payload capacity
- 12 minute estimated flight time
- 450 mm rotor to rotor wing span

Figure 31: DJI Flamewheel F450 with onboard Odroid-UX4 SBC and Optitrack ridged body markers positioned on the GPS Stand.

5.2 Control and communications using ROS

Robot operating system is a framework for communications for sensors and robots. It in an open source tool with wide community support for innumerable types of robotics applications. ROS was chosen for its sensor and platform agnosticism. It works through the use of nodes and topics. Nodes can either publish to a topic, subscribe to a topic or both. In a very simple example shown in **Figure 32,** a publisher will provide data, usually from a sensor of some kind like a lux sensor reading or motion capture information, and publish that data to a topic. A subscriber will then subscribe that topic to use that information in some way.
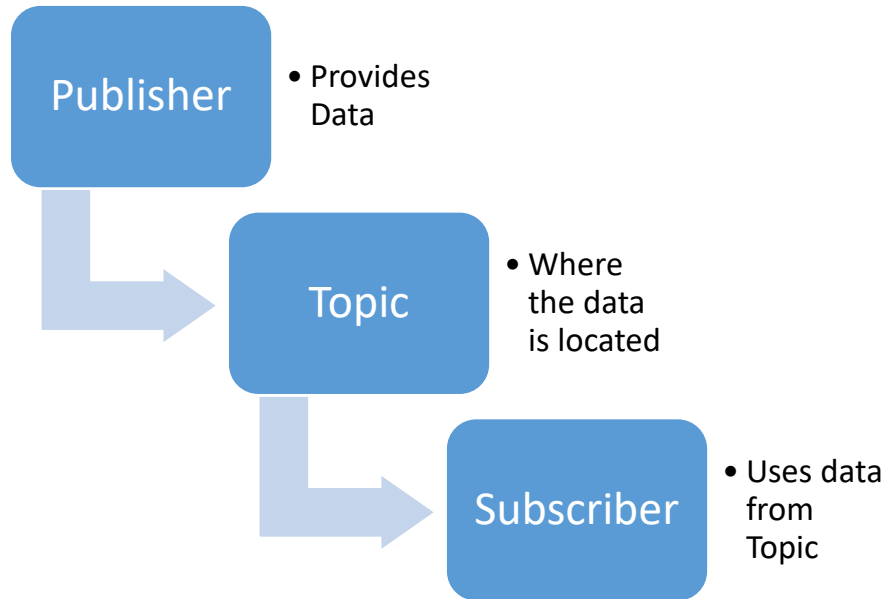
Figure 32: Basic Robot Operating System (ROS) framework

5.3 Flight Testbed

The flight volume at the Intelligent structures and Controls Laboratory is 20x14x16ft in volume. It is outfitted with an OptiTrack motion capture system to allow real time feedback of the position and orientation of objects within the flight volume at 120hz. The system uses 8 infrared cameras with a ring of infrared LEDs. The LEDs illuminate high gain reflective markers that are placed on any rigid body enabling it to be tracked with sub-millimeter accuracy within the flight volume. **Figure 33** shows the OptiTrack Camera, flight volume, and the reflective markers used for the motion capture system.
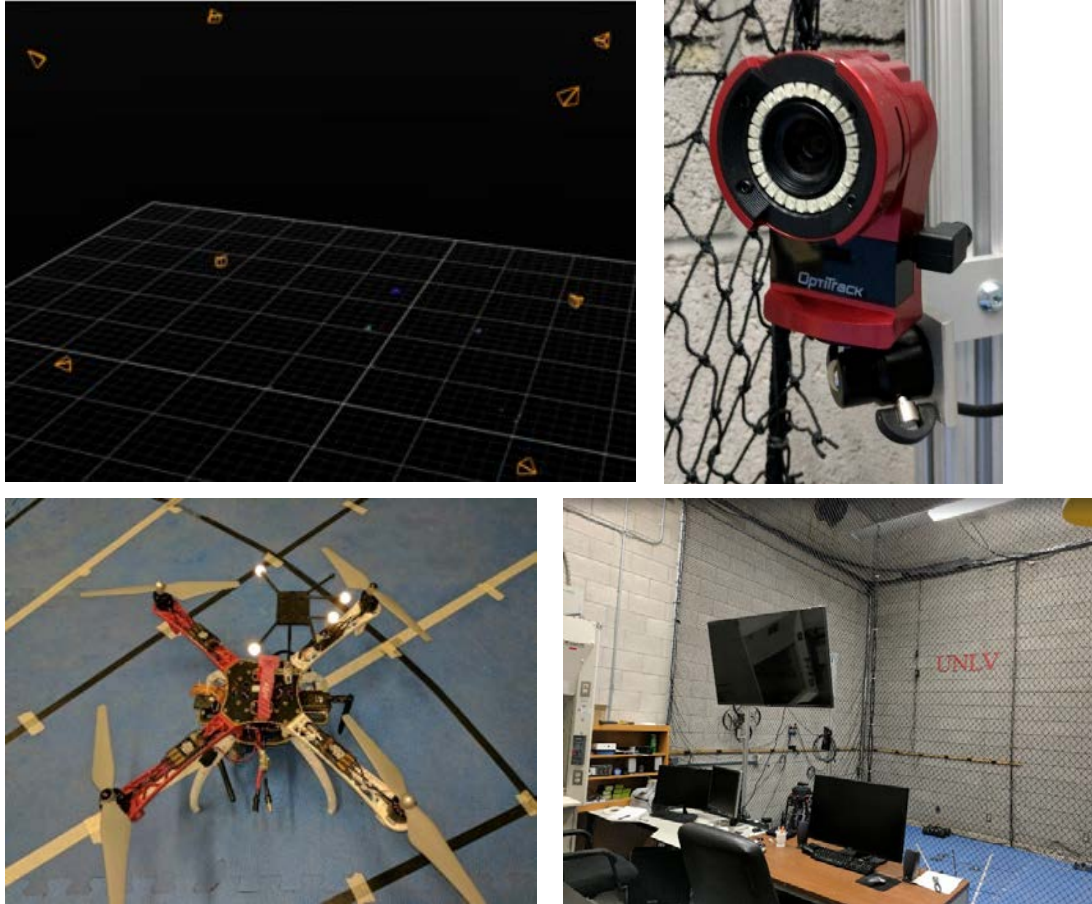
Figure 33: Motion capture flight volume 20x14x16'

5.4 Experimental contour mapping

5.4.1 Light sensor and source setup

Because it is not practical to test using a real radiation source, a light source is used as an analog to a radiation source. A test showed that the this parituclair light bulb was iosmetric enough to consider it an analog as long as the light source was kept perpediculair to the ground plane. Each UAS is outifited with an arduino, light sensor, and Xbee shown in **Figure 34**.
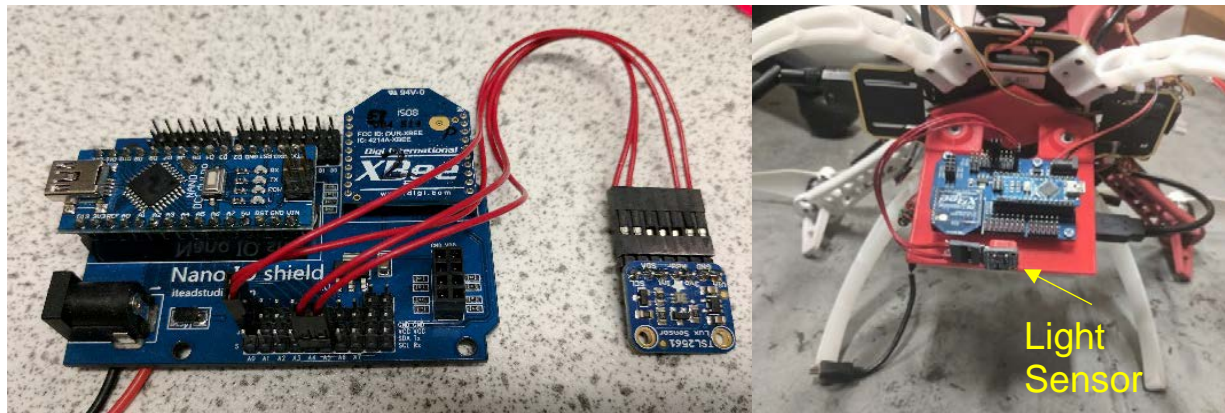
Figure 34: Arduino based mesh networked Lux sensor.

It was necessary to verify the readings of the light sensor that would be onboard each UAS. To do that, a polar grid was laid out with marks at every foot from 0 - 8 ft and at every 11.25 degrees from 0 to 90 degrees. This grid is shown in **Figure 35.** The light source was placed at (0, 0º) so that the light was shining along the 0º axis. Then sensor was then moved to each coordinate while the sensor and light source stayed parallel to each other to simulate how the sensor would be oriented to the source when it was onboard a UAS.

5.4.4 gradient measurement error

In order to verify the computer model of gradient estimation, the UAS swarm was placed upside down roughly equiangular around the center of the flight volume. The UAS were placed at 0.5m radius away from the center. The light source, acting as a radiation analog, was moved around the swarm in a circle at a 0.5m radius concentric with the swam. Data was captured through the wireless sensor network fed to the gradient estimation algorithm located on the base station computer. The light source and each UAS are identified in the OptiTrack software as a ridged body so the position of the light w.r.t. the swarm could be compared to the computed gradient estimation. The experimental setup is shown in **Figure 36.**

39
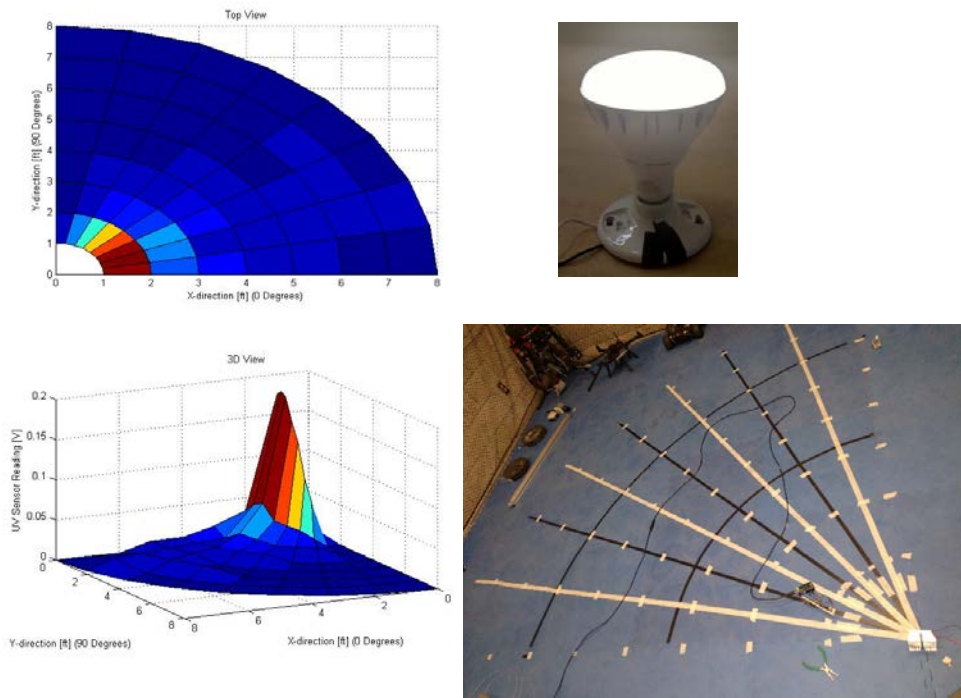
Figure 35: Sensor verification measurement with angle and distance markers. Sensor was held parallel to light source during measurements as would happen in flight.
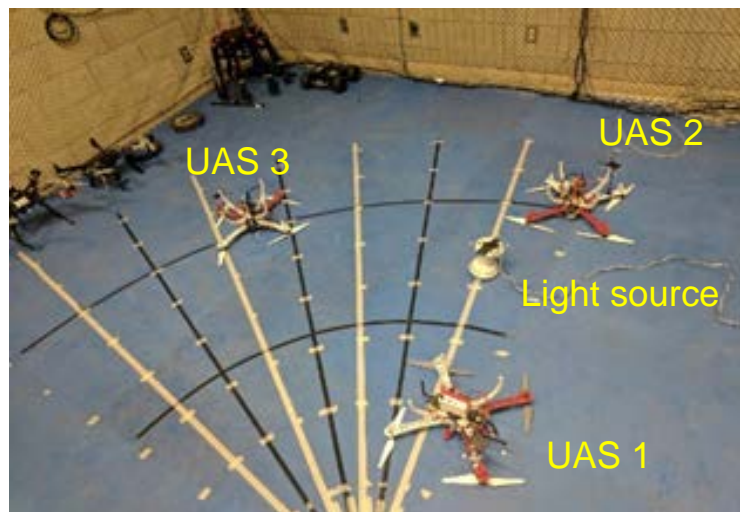
Figure 36: Experimental setup for gradient error testing.

Figure 37 shows that the experiment does agree with the experiment. In the experiment, there are higher and lower data points in comparison to the simulation due to imperfect angular

40

spacing around the circle that they were placed. The spacing between UAS 1 and UAS 2 is less than the ideal $\frac{2\pi}{3}$ and so the error in the experiment us smaller than the simulation. The spacing between UAS 2 and UAS 3 is larger than $\frac{2\pi}{3}$, therefore the error measured is larger than the simulation.
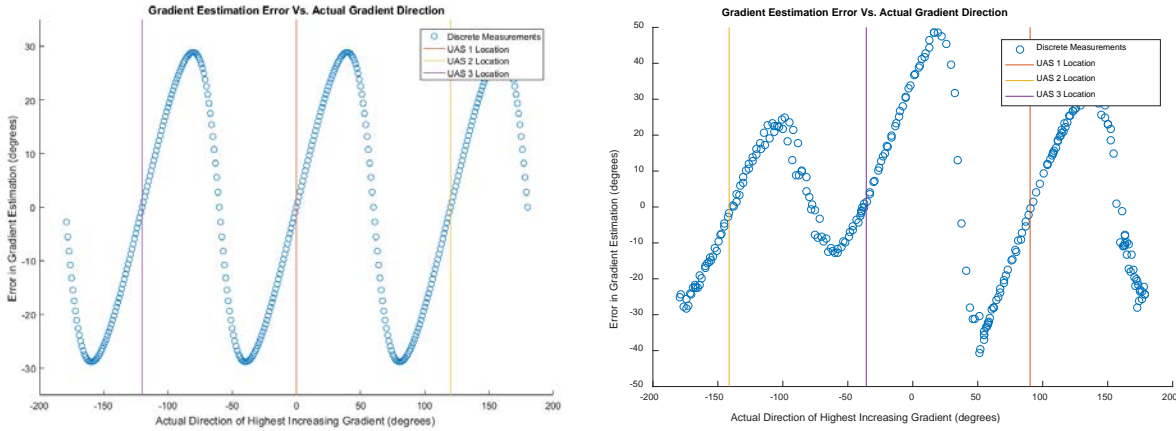
Figure 37: Gradient estimation error experiment.

5.4.4 Source seeking behavior

Due to space constraints using the DJI Flamewheel F450 UAS in the flight volume, source seeking was used to test the light sensors and gradient estimation algorithm rather than contour mapping. The light source was placed on a movable dolly within the flight volume moved along the x-axis to show that the gradient detection is successful in determining the direction of the source giving sensor values from the wireless sensors located on each UAS. The swarm was restricted to move along the x-axis and the reference position generation was bound to ±0.5 m. This was chosen to minimize risk of the swarm crashing into the sides of the flight volume.

41

Chapter 6: Results and Discussion

Experimentation

To demonstrate contour mapping's effectiveness, Crazyflie UAS were used. A virtual source was used instead of a radiative source or source analog. This method was chosen because, while a Crazyflie swarm is small enough to accomplish contour mapping within the given flight volume, the payload carrying capability of the UAS doesn't allow for a real sensor. OptiTrack tracked the position of the source and each UAS swarm agent. The "source strength" detected by each UAS to be used by the gradient estimation was $\frac{1}{r^2}$ with r being the distance from the source to each respective UAS. **Figure 38** shows the UAS swarm (circled in green) and virtual source (circled in red) along with an overhead plot of their position (x,y) to more easily see where the UAS are in relation to the source.
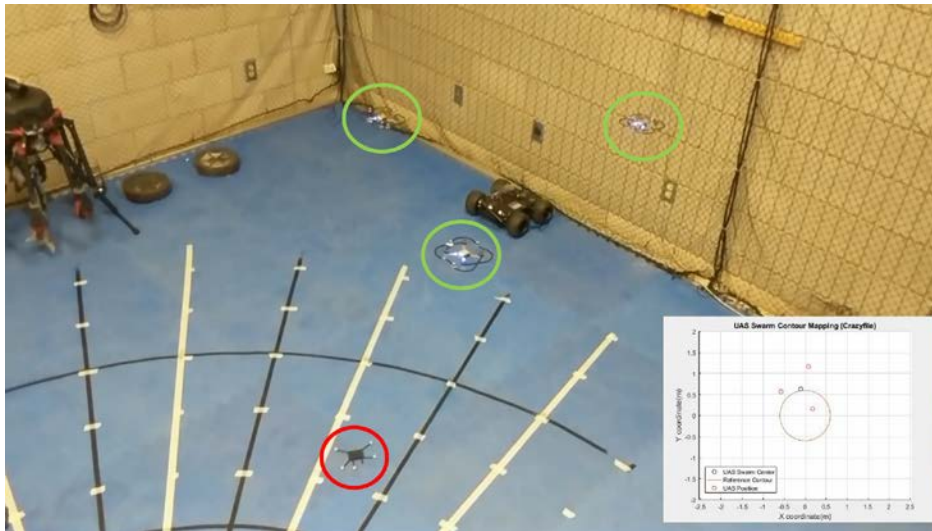
Figure 38: Crazyflie 2.0 UAS (circled in green) swarm mapping around the rigid body on the ground identified by the OptiTrack ridged body marker (circled in red) .

The experimental results from the contour mapping is shown in **Figure 39.** The trajectory of the center of the swarm mapped the desired contour to within ±0.1m.
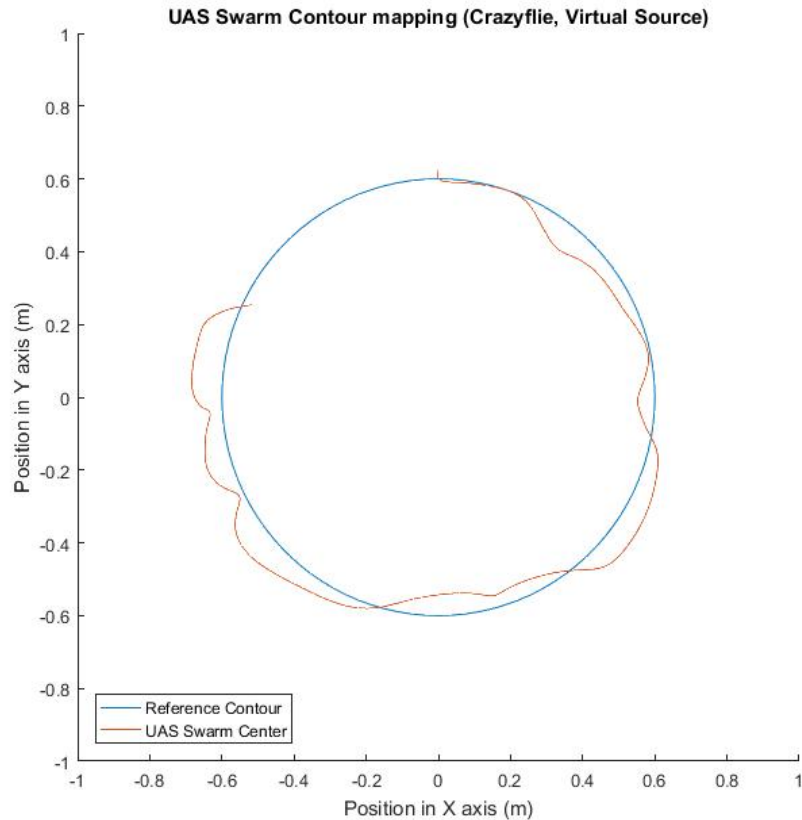
Figure 39: Path the UAS swarm traveled mapping the contour of a virtual source.

To validate both source seeking behavior and the wireless mesh sensor network with the light sensors located on each UAS, an experimented demonstrating source seeking is shown in **Figure 40.** The light source was placed on a rolling platform to allow for moving of the source to show that the swarm can track the position of the light when it is moved. The tracking of the light source and all UAS platforms was done via the OptiTrack motion capture.

43
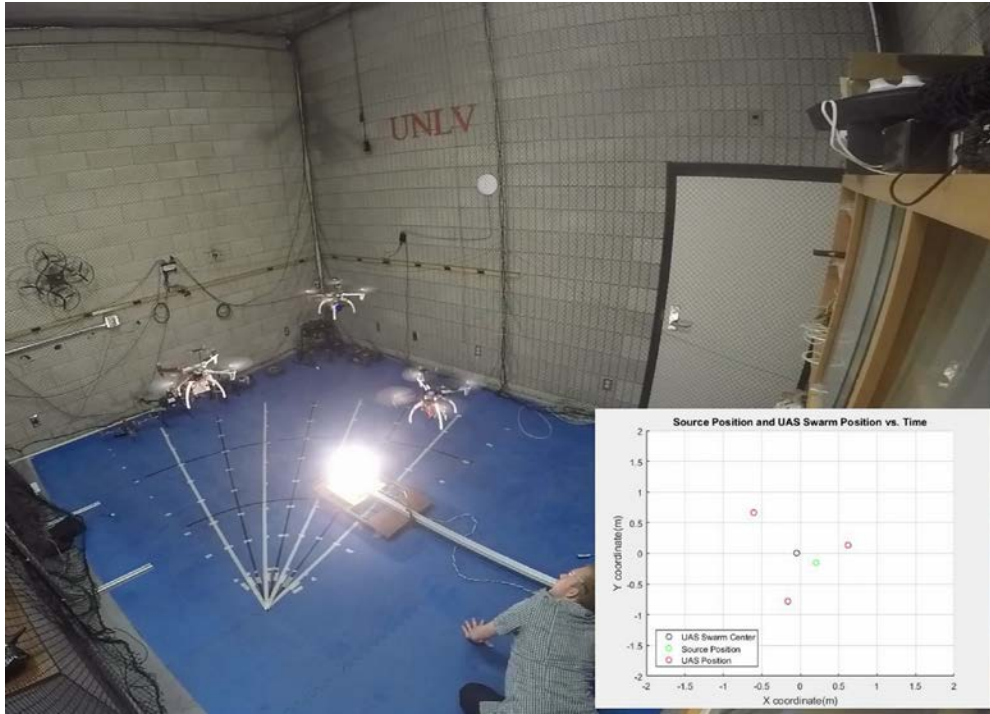
Figure 40: UAS Swarm demonstrating Source seeking behavior using light source and lux sensors.

Figure 41 shows the experimental results of the source seeking experiment using the DJI Flamewheel F450. Plotted is the position of the light source vs the position of center of the swarm dictated by the source seeking algorithm. The swam oscillates around the light's position because the there is a constant velocity defined for the swarm center so even if the swarm is infinitesimally close to the source, the swarm will still travel at full speed in the direction increasing gradient and overshoot the actual position of the source. Ultimately, the swarm was successful in seeking the source even when the source was moving and validated the wireless sensor network, analog source, and gradient estimation algorithm.

44
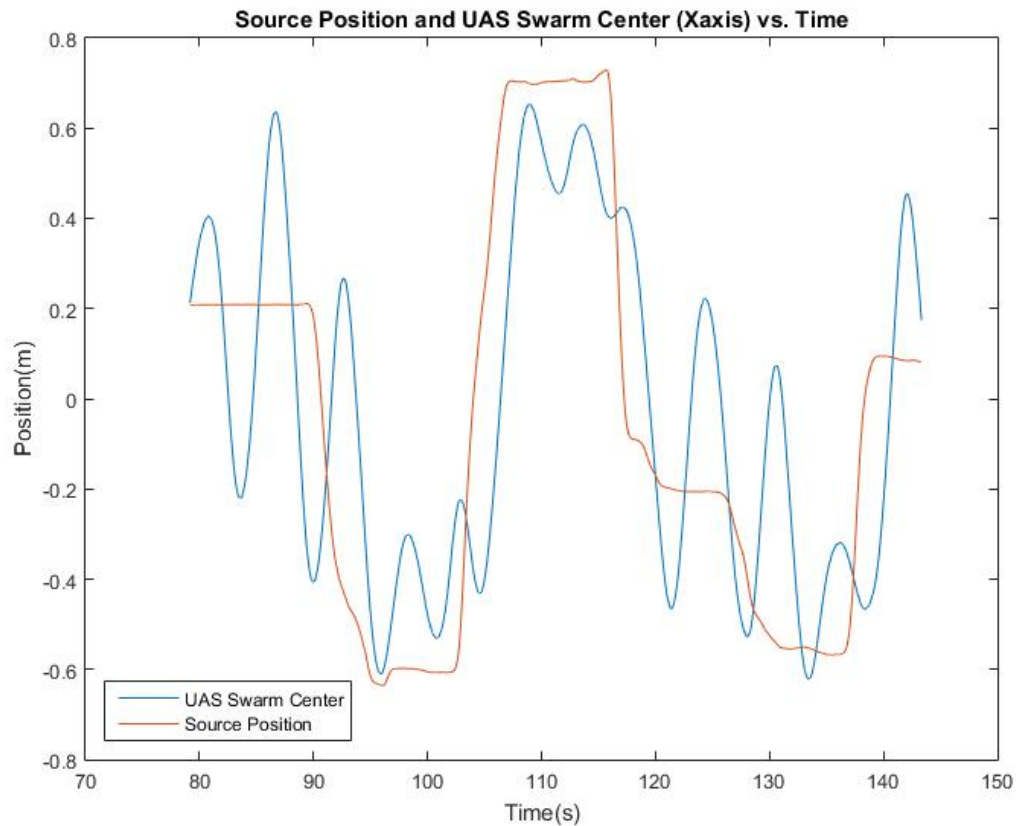
Figure 41: Source and Swarm position vs. Time.

In conclusion, a method of contour mapping and source seeking by a UAS swarm with onboard radiation spectrometers was developed. A rotating circular formation of UAS are used to detect the direction of steepest gradient which is then used to determine the overall heading of the swarm. The contour mapping algorithm was first simulated, with the assumption of a $1/R^2$ radiation model, within Matlab and Simulink to verify its validity. The simulation considered the dynamics of the UAS and an adaptive rotation rate algorithm was implemented to reduce the overall path length that each UAS would have to fly. A more realistic simulated radiation field was generated using MCNP that incorporated scattering and attenuation of the radiation signature due to obstacles. Using a swarm of three UAS, a reference contour of the MCNP generated field

45

was successfully determined using the contour mapping algorithm. Both source seeking and contour mapping algorithms were successfully verified experimentally within the motion capture flight volume. Ultimately these techniques can reduce the time necessary to survey an unknown environment contaminated with a stationary or slowly moving radiative source to assist in overall situational awareness.

Future Work

An outdoor testbed is currently being outfitted with the necessary equipment to validate much bigger UAS for use with the same algorithms presented in this work. The outdoor facility shown in **Figure 42** has mesh netting for a ceiling so that Real Time Kinematic (RTK) GPS can be used as a viable option for guidance and position feedback. In addition, an OptiTrack Motion capture system for use outdoors is being outfitted for when more precise positioning and guidance is necessary.

Figure 42: Outdoor flight volume for use with GPS capable UAS.

46

Bibliography

[1]   M. Buchroithner, "Gomantong Congress Paper 2013 AND AUTONOMOUS DRONE SURFACE-HOTOGRAMMETRY," no. October, pp. 1–4, 2015.

[2]   C. C. Haddal and J. Gertler, "CRS Report for Congress Homeland Security: Unmanned Aerial Vehicles and Border Surveillance Specialist in Immigration Policy Specialist in Military Aviation," 2010.

[3]   N. Nigam and I. Kroo, "Persistent Surveillance Using Multiple Unmanned Air Vehicles," *Aerosp. Conf. 2008 IEEE*, pp. 1–14, 2008.

[4]   S. Bashyal and G. K. Venayagamoorthy, "Human swarm interaction for radiation source search and localization," *2008 IEEE Swarm Intell. Symp. SIS 2008*, 2008.

[5]   P. Boccardo, F. Chiabrando, F. Dutto, F. G. Tonolo, and A. Lingua, "UAV deployment exercise for mapping purposes: Evaluation of emergency response applications," *Sensors (Switzerland)*, vol. 15, no. 7, pp. 15717–15737, 2015.

[6]   Y. Sato *et al.*, "Remote radiation imaging system using a compact gamma-ray imager mounted on a multicopter drone," *J. Nucl. Sci. Technol.*, vol. 3131, no. October, pp. 1–7, 2017.

[7]   E. T. Brewer, "Autonomous Localization of 1 / R 2 Sources Using an Aerial Platform," Virginia Tech, 2009.

[8]   R. Sepulchre, D. A. Paley, and N. E. Leonard, "Stabilization of planar collective motion: All-to-all communication," *IEEE Trans. Automat. Contr.*, vol. 52, no. 5, pp. 811–824, 2007.

[9]   N. E. Leonard, D. a. Paley, F. Lekien, R. Sepulchre, D. M. Fratantoni, and R. E. Davis, "Collective Motion, Sensor Networks, and Ocean Sampling Collective Motion, Sensor Networks, and Ocean Sampling," *Proc. IEEE*, vol. 95, no. 1, pp. 48–74, 2007.

[10] R. L. Raffard, C. J. Tomlin, S. P. Boyd, and A. P. Formulation, "Distributed Optimization for Cooperative Agents : Application to Formation Flight," *IEEE Conf. Decis. Control*, pp. 2453–2459, 2004.

[11] J. A. Marshall, M. E. Broucke, and B. A. Francis, "Formations of vehicles in cyclic pursuit," *IEEE Trans. Automat. Contr.*, vol. 49, no. 11, pp. 1963–1974, 2004.

[12] P. Ogren, M. Egerstedt, and X. Hu, "A control Lyapunov function approach to multiagent coordination," *Robot. Autom. IEEE …*, vol. 18, no. 5, pp. 847–851, 2002.

[13] L. B. Arranz, A. Seuret, and C. C. De Wit, "Translation control of a fleet circular formation of AUVs under finite communication range," *Proc. IEEE Conf. Decis. Control*, pp. 8345–8350, 2009.

[14] B. J. Moore and C. Canudas-de-Wit, "Source seeking via collaborative measurements by a circular formation of agents," *Am. Control Conf. (ACC), 2010*, 2010.

[15] R.A. Cortez and H.G. Tanner, "Radiation Mapping Using Multiple Robots," *Trans. Am. Nucl. Soc.*, vol. 99, pp. 157–159, 2008.

[16] J. Han and Y. Chen, "Multiple UAV formations for cooperative source seeking and contour mapping of a radiative signal field," *J. Intell. Robot. Syst. Theory Appl.*, vol. 74, no. 1–2, pp. 323–332, 2014.

[17] M. A. Mariscotti, "A method for automatic identification of peaks in the presence of background and its application to spectrum analysis," *Nucl. Instruments Methods*, vol. 50, no. 2, pp. 309–320, 1967.

[18] S. Uryasev, "Derivatives of probability functions and some applications," *Ann. Oper. Res.*, vol. 56, no. 1, pp. 287–311, 1995.

[19] P. Ogren, E. Fiorelli, and N. E. Leonard, "Cooperative control of mobile sensor networks:

Adaptive gradient climbing in a distributed environment," *IEEE Trans. Automat. Contr.*, vol. 49, no. 8, pp. 1292–1302, 2004.

[20] W. Gander, G. H. Golub, and R. Strebel, "Least-Squares Fitting of Circles a N D Ellipses," *Gene*, vol. 34, no. July, pp. 558–578, 1994.

[21] B. A. Boukamp, "A nonlinear least squares fit procedure for analysis of immittancs data of electrochemical systems," *Solid State Ionics*, vol. 20, pp. 31–44, 1986.

[22] T. Goorley, "Initial MCNP6 Release Overview," *Nucl. Technol.*, vol. 180, no. 3, pp. 298–315, 2012.

[23] W. Honig, C. Milanes, L. Scaria, T. Phan, M. Bolas, and N. Ayanian, "Mixed reality for robotics," in *IEEE International Conference on Intelligent Robots and Systems*, 2015, vol. 2015–Decem, pp. 5382–5387.

Curriculum Vitae

Zachary J. Cook   –   cookz2lal@gmail.com

EDUCATION

2015 – Present2017 , University of Nevada, Las Vegas Master of Science in Mechanical Engineering with focus in Dynamics and Automatic Controls

2007 - 2015 ,University of Nevada, Las Vegas Bachelors of Science in Mechanical Engineering (Engineering GPA 3.8)

2007 - Las Vegas Academy for Performing Arts and International Studies Advanced Diploma (Double Major Jazz and Concert Band)

WORK EXPERIENCE

Development and Production of Prototype Card Shuffler   June 2015 – July 2016

Worked as part of a three-person team to invent and produce a working prototype for a single deck card shuffler for poker games. This Project was funded by Shark Trap Gaming & Security Systems LLC, in cooperation with UNLV. A patented working prototype was delivered.

50

Graduate Research Assistant (UNLV)   Sept 2015 - Present

      Intelligent Systems and Controls Lab - Developing drone platforms and flight algorithms for UAV swarms to autonomously locate sources of gamma and neutron radiation. The swarm algorithms were first simulated within Matlab/Simulink to ensure viability and then experimentally tested within a motion capture feedback flight volume. Ultimately these methods will be used to help first responders dramatically reduce the time it takes to determine safe boundaries for humans in a radiological disaster situation.

      Developed Autonomous navigation and obstacle avoidance algorithms used for both ground and air vehicles. Robot Operating system was used as a framework to interface many independent systems on the vehicles including Hokuyo LIDAR, Light sensors, Ultrasonic Sensors, Stereo Infrared Cameras, Motor controllers and microcontrollers. The computation was done by single board Linux computers (OdroidUX4) running onboard the vehicles.

Drafting/Mechanical Engineer in Training   Jan - Sept 2015

      HPA Consulting Engineers- Las Vegas, NV – Mechanical, Plumbing, and Electrical drafting. Responsibilities include the sizing of different types of mechanical equipment (HVAC/Plumbing) for new and retrofit construction and completing building plans in adherence to strict deadlines.

Undergraduate Research Assistant (UNLV)   April 2014 - Jan 2015

51

Developed, ran, and maintained biomechanical experiments involving measuring the mechanical properties of ex-vivo human tissue that is affected by the condition of Pelvic Organ Prolapse.

Designed, modified and produced a low cost 3D printed prosthetic hand for use by children. This project was a collaborative effort between many entities including UNLV, Touro University, Matt Smith Physical Therapy, and the Las Vegas Syn Shop.

Professional Musician   2006 - 2012

Various venues including the Hard Rock Café, 2007 Spike TV Video Game Awards and community events, teaching and tutoring trombone and baritone/euphonium.

Customer Service/Cashier   May – Aug 2011

Cinemark – South Point, Las Vegas, NV   - Customer Service/Cashier/Point of Service Machine

Electrical Yard Foreman Assistant - Paid Summer Internship   May – Aug 2006

Magna Electric, Las Vegas, NV - Assisted Yard Foreman in installation of municipal lighting systems and street light maintenance.

SKILLS AND ABILITIES

- Proficient in SolidWorks, MATLAB, Robot Operating System (ROS), Autocad MEP and LabView.

- Knowledge of CAM and Machining Processes.

- Programing experience in C, C++ and Python.

- Knowledge of Electronics for the Purposes of Prototyping (Arduino, and Single board Computers)

- Word, Excel and Power Point.

- Experience in Composites for use with Drones.

- FEA and CFD analysis particularly within SolidWorks and Ansys.

- MATLAB- Extensive time spent developing image/video processing programs.

- Leadership and Communication (Project Management) – Led a team of engineering students in designing and fabricating a human powered vehicle.

- Extensive knowledge and experience in 3-D printing, specifically fused deposition modeling.

- Proficient in the use of Motion Capture for the purpose of robotics (Optitrack).

- Helped organize and run NeCoTIP Engineering Summer Institute, where elementary school teachers went through a multi-day workshop learning the principals of engineering and design.

Patents (Inventor Credit):

Automatic Card Shuffler

Patent# 9,573,047, Issued February 21, 2017

Multi-Deck Automatic Card Shuffler Configured to Shuffle Cards for a Casino Table Game Card Game such as Baccarat

Patent Application #15/371,125, Filed December 6, 2016

Scientific Papers:

Journals:

Z. Cook, S Prisbastami, B. O'Toole, M. Trabia, "Practical and Inexpensive Procedure to Measure Mechanical Properties of Vaginal Tissue", in the *Journal of Neurourology and Urodynamics*. Vol. 30 Page S8, 2015.

Conferences:

Z. Cook, L. Zhao, J. Lee, W. Yim, "Unmanned Aerial Vehicle for Hot-spot Avoidance with Stereo FLIR Cameras", in *Proceedings of the 12th International Conference on Ubiquitous Robots and Ambient Intelligence 2015*, Goyang, Republic of Korea, Oct. 2015

Z. Cook, L. Zhao, J. Lee, W. Yim, "Unmanned Aerial Systems for First Responders", in *Proceedings of the 12th International Conference on Ubiquitous Robots and Ambient Intelligence 2015*, Goyang, Republic of Korea, Oct. 2015

J. Y. Lee, J. Hartman, Z. Cook, J. S. Lee, W. S. Yim, A. Barzilov, "Development of Plug– and – Play Interchangeable Components for Unmanned Aerial System with Mobile Manipulation Capability", in *Proceedings of the 2016 ANS Winter Meeting and Technology Expo*, Las Vegas, NV, USA, Nov. 2016

Z. Cook, J. Y. Lee, J. Hartman, W. Yim, A. Barzilov, "Contour Mapping Based Radiation Source Localization by UAS Swarm", in *Proceedings of the 2016 ANS Winter Meeting and Technology Expo*, Las Vegas, NV, USA, Nov. 2016

J. Y. Lee, Z. Cook, A. Barzilov, W. Yim, "Control of an Aerial Manipulator with an On-Board Balancing Mechanism", in *Proceedings of the ASME 2016 International Mechanical Engineering Congress and Exposition*, Phoenix, AZ, USA, Nov. 2016

COMMUNITY AND PROFESSIONAL INVOLVEMENT

- American Society of Mechanical Engineers (ASME) – 2015 Project Manager (Human Powered Vehicle)

- Society of Automotive Engineers (SAE)- Part of the team to develop the 2015 UNLV BAJA Vehicle

- American Nuclear Society (ANS) member

- President of UNLV Swing Club

- UNLV Jazz Band – 2007 to 2010